INL/RPT-22-67366

Preliminary Pilot-scale Study and Techno-economic Analysis of Chemical Heat Pump with Conventional Nuclear Reactors

2022

Internship Report

Aman Gupta
Idaho National Laboratory, University of Idaho

Dr. Piyush Sabharwall
Idaho National Laboratory

Dr. Vivek Utgikar
University of Idaho

Idaho National Laboratory

INL is a U.S. Department of Energy National Laboratory operated by Battelle Energy Alliance, LLC

DISCLAIMER

This information was prepared as an account of work sponsored by an agency of the U.S. Government. Neither the U.S. Government nor any agency thereof, nor any of their employees, makes any warranty, expressed or implied, or assumes any legal liability or responsibility for the accuracy, completeness, or usefulness, of any information, apparatus, product, or process disclosed, or represents that its use would not infringe privately owned rights. References herein to any specific commercial product, process, or service by trade name, trade mark, manufacturer, or otherwise, does not necessarily constitute or imply its endorsement, recommendation, or favoring by the U.S. Government or any agency thereof. The views and opinions of authors expressed herein do not necessarily state or reflect those of the U.S. Government or any agency thereof.

INL/RPT-22-67366

Preliminary Pilot-scale Study and Techno-economic Analysis of Chemical Heat Pump with Conventional Nuclear Reactors

Internship Report

Aman Gupta
Idaho National Laboratory, University of Idaho
Dr. Piyush Sabharwall
Idaho National Laboratory
Dr. Vivek Utgikar
University of Idaho

2022

Idaho National Laboratory
Idaho Falls, Idaho 83415

http://www.inl.gov

Prepared for the
U.S. Department of Energy
Office of Nuclear Energy
Under DOE Idaho Operations Office
Contract DE-AC07-05ID14517

Page intentionally left blank

ABSTRACT

The energy economy is continually evolving, particularly in terms of primary energy sources, their conversions to useful forms such as electricity and heat, and their utilization in different sectors, in response to socio-political factors. Because nuclear source is clean and non-carbon-emitting energy source, it is crucial to consider its role in the evolution of the energy economy. A pilot-scale study was conducted for Chemical Heat Pump (ChHP) system at three different scales (25-, 100-, and 1000-kW thermal outputs) using steady state thermal model. To establish the viability of selling heat rather than electricity alone, techno-economic analysis was undertaken for advanced Small Modular Reactor (SMR), and SMR paired with varied thermal output ChHP systems was referred to as the nuclear hybrid energy system (NHES) in this study. Using the U.S. Energy Information Administration statistics, pricing for electricity and natural gas were anticipated for U.S. regions (California, Northwest, Midwest, Southwest, New England, and PJM – Pennsylvania, New Jersey, and Maryland). Based on thermal output from ChHP, advanced SMR with 100 MW_{th} and four alternative NHES scenarios were explored, namely 50-, 10-, 5-, and 1-MW_{th}. Net present value, payback period, discounted cash flow return, and levelized cost of energy were evaluated for all scenarios. Based on the economic analysis, selling heat to high-temperature industrial processes is more profitable compared to selling electricity only. Higher carbon taxes showed significant improvement in economic parameters for NHESs. Providing heat to high-temperature industries could be beneficial, helping to reduce the greenhouse gas emissions by slashing the fossil fuel consumption.

ACKNOWLEDGEMENTS

This research is being performed using the funding received from DOE office of Nuclear Energy's Nuclear Energy University Program under Awards Number DE-NE0008775. The authors would like to thank Dr. Brian M. Fronk and Paul D. Armatis from Oregon State University for their valuable feedbacks, comments, and edits for this work.

Page intentionally left blank

CONTENTS

FIGURES

TABLES

Page intentionally left blank

NOMENCLATURE

$\bar{A}$	average annuity	\$
A	annuity	\$
A_{HT}	heat transfer area	m^2
C	rate	-
CC	contingency cost rate	-
CF	capacity factor	-
c_0	costs	\$
$DCFR$	discounted cash flow rate of return	-
$DD\&E$	detailed design and engineering rate	-
d	depreciation rate	-
E	energy	MWh
$Fuel_{spec}$	specific fuel cost	$\$\ MW_e^{-1}$
h_c	convective heat transfer coefficient	$W\ m^{-2}\ K^{-1}$
ID	inner diameter	m
i	discount rate	-
k	thermal conductivity	$W\ m^{-1}\ K^{-1}$
$LCOE$	levelized cost of energy	$\$\ MW^{-1}\ h^{-1}$
L	length	m
NPV	net present worth	\$
Nu	Nusselt number	-
N	time period	yr
n	number or magnitude	-
$O\&M_{fix}$	fixed operations and maintenance	$\$\ MW_e^{-1}yr^{-1}$
$O\&M_{spec}$	specific operation and maintenance	$\$\ MW_e^{-1}$
OCC	overnight capital cost	$\$\ kW_e^{-1}$
OD	outer diameter	m
PBP	payback period	yr
Pr	Prandtl number	-
PWF	present worth factor	-
p	portion	-
$\dot{Q}$	heat transfer rate	W, MW
Re	Reynolds number	-
r	rate	-
R_c	thermal contact resistance	$m^2K\ W^{-1}$
rec	recovered cost from salvaged equipment	\$
SP	selling price of utility	$\$\ MW^{-1}\ h^{-1}$
SCC	specific capital cost	$\$\ kW_e^{-1}$
₸	annual investment	\$
T	temperature	°C
t	thickness	m
U	overall heat transfer coefficient	$W\ m^{-2}\ K^{-1}$
u	velocity	$m\ s^{-1}$
V_{bed}	volume of bed	m^3
$\dot{V}$	volumetric flow rate	$m^3\ s^{-1}$
V	fixed capital investment	\$

WACC	weighted average capital cost	-

Greek Letters

Δ	change or difference	-
η	first law thermodynamic efficiency	-
μ	viscosity	kg m^{-1} s^{-1}
Φ	tax rate	-
ρ	density	kg m^{-3}

Subscript/superscript

bed	bed
c	construction
cf	annual cash flow
d	debt
de	dehydration
eq	equity
e	electricity
f	fluid
ht	heat
hy	hydration
inf	inflation
j	plant operation year index
k	plant operation year index
th	thermal
v	investment

ACRONYMS

CF	capacity factor
ChHP	Chemical Heat Pump
DCFR	discounted cash flow return
FBR	fluidized bed reactor
FOAK	first-of -a-kind
GHG	greenhouse gas
HTF	heat transfer fluid
IAEA	International Atomic Energy Agency
IES	Integrated Energy Systems
IRR	internal rate of return
LCOE	levelized cost of energy
MACRS	Modified Accelerated Cost Recovery System
NHES	Nuclear Hybrid Energy System
NOAK	nth-of-a-kind
NPV	net present value
O&M	operations and maintenance
OCC	overnight capital cost
PBP	payback period
PJM	Pennsylvania, New Jersey, and Maryland
SMR	Small Modular Reactor
TCES	thermochemical energy storage system
TEA	techno-economic analysis
WACC	weighted average cost of capital

Page intentionally left blank

1. INTRODUCTION

The world faces a new challenge in the twenty-first century—substantially lowering greenhouse gas emissions while simultaneously providing energy access and economic opportunity to billions of people. During the 2021 United Nations Climate Change Conference of the Parties (COP26), 137 countries committed to net-zero, carbon neutrality or being climate-neutral, including China, United States, and India. To have a major impact on greenhouse gas (GHG) emissions, non-electric energy sectors' (industry, commercial, residential, and transportation) carbon footprint must be considered to achieve long-term emission reduction targets. Growth of the nuclear power sector can help realize the goal of a reliable, carbon emission free energy mix. While nuclear power is technologically mature and reliable, the economic stability of nuclear power has been challenged due to an in influx of highly incentivized and intermittent renewable energy sources. High penetration of solar and wind energy into the power grid drops the value of electricity to low or even negative prices at certain times of day and year, reducing the nuclear power plant viability [1]. This significantly increases the payback period and financial risk of investment in nuclear power plants, despite their ability to provide reliable base-load power.

1.1. Nuclear Energy Current Status

According to the Nuclear Energy Institute [2], the United States avoided more than 476 million metric tons of carbon dioxide emissions in 2019, which is equivalent to removing 100 million cars from the road and more than all other clean energy sources combined. Contributing massive amounts of carbon-free power, nuclear energy produces more electricity on less land than any other clean-air source. A typical 1,000-megawatt nuclear facility in the United States needs a little more than 1 square mile to operate. Wind farms require 360 times more land area to produce the same amount of electricity and solar photovoltaic plants require 75 times more space.

Cost has been the primary issue facing the nuclear industry for over 20 years. When explaining the relatively limited expansion of nuclear power, the recent MIT Future of Nuclear report stated the fundamental problem is cost [3]. The nuclear power plant fleet in the United States was profitable during the most of the 2000s: their capital costs having been largely amortized over previous decades, and their operational costs were cheap compared with the relatively high cost of fossil and renewable alternatives. Utilities embarked on a flurry of market-driven nuclear power plant purchases, power uprates, and license extensions as they attempted to maximize the value of their nuclear assets.

Current nuclear power reactors produce usable energy in the form of heat at modest temperatures (approximately 300°C); this heat is then converted to electricity using a steam turbine power cycle. In advanced nuclear reactors (so-called Generation-IV designs), the primary energy product is again heat, but planned to be delivered at much higher temperatures (500°C–800°C). These higher operating temperatures offer a potential opportunity for nuclear high-temperature reactor technology to provide useful process heat directly in industrial applications.

The International Atomic Energy Agency (IAEA) formally defines small modular reactors (SMRs) as nuclear reactors capable of producing less than 300 MW_e of power [4]. Microreactors can supply anywhere from 1 to 20 MW_e, thus producing less than 7% of the power output by SMRs, less than 0.7% of existing commercial reactors, and are transportable, and often self-adjusting. In the United States, very few utility companies have the required equity to finance the large upfront capital costs associated with reactors over 700 MW_e. Therefore, many new SMR designs are being seriously considered and are in the design, research and development, or licensing stages.

1.1 Integrated Energy System

Researchers have been attracted by Integrated Energy Systems (IES) in recent years due to their potential to reduce GHG emissions, increase energy efficiency, improve electrical grid dependability, and enhance energy economics as shown in Figure 1. IES are collaboratively controlled systems that dynamically apportion thermal and/or electrical energy to promote the production of various energy products while also providing responsive generation to the power grid. Multiple subsystems make up an IES, which may or may not be geographically co-located [5–6]. To realize the benefits of IES with the current reactor fleets by providing process heat and improving economics, selection and development of a complimentary temperature upgrading technology is necessary. Multiple distinct energy sources operate behind a single grid link in this case. Thermal energy can be used to generate power, be stored, or be used in industrial thermal processes. In response to changing electric market conditions, this energy distribution can be modified to maximize the value of the IES. Solar thermal and nuclear power are becoming less appealing to investors as the price of electricity fluctuates due to the arrival of renewable energy sources such as solar photovoltaic panels and wind turbines. Solar thermal and nuclear facilities do minimize greenhouse gas emissions, but they come with high upfront investments that are difficult to recover rapidly in a fluctuating energy market. While thermal storage is a component of the solution, there is also an opportunity to sell heat instead of power when it is more profitable. Several heat sources with zero GHG emissions can be employed for industrial heating.

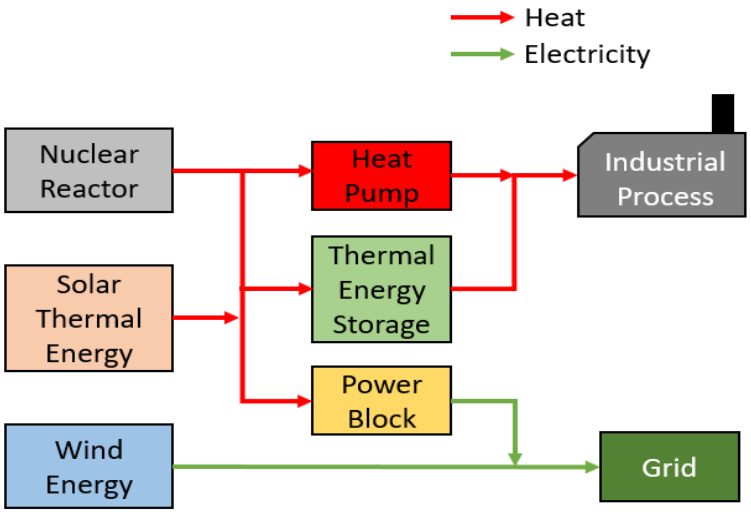

Figure 1. Example of Integrated Energy Systems.

McMillan et al. gathered data on thermal energy consumption and CO_2 emissions for high-temperature thermal process businesses in the United States in 2016 [7]. They discovered that boilers or combined heat and power accounted for 70% of the 51 TBtu consumed in the U.S. industrial sector in 2014, while direct process heating accounted for another 24%. Because fossil fuels (mainly natural gas) are readily available, affordable, and simple to utilize, they are commonly used to generate the requisite high-temperature heat. Instead of fossil fuels, using nuclear or renewable thermal energy for these applications can significantly reduce GHG emissions. This also opens the possibility of using energy sources other than electricity, which is not always feasible due to fluctuating electricity prices. The use of low-carbon energy sources could be improved by combining energy storage and better-integrated varied energy markets. Conventional nuclear reactors operate at 300–325°C, whereas the high-temperature thermal industrial process typically requires heat at greater than 550°C, as shown in Figure 2. To address the temperature mismatch, heat pumps are used between the nuclear power plant and the desired high-temperature thermal industries. Heat pump technologies are preferable to other alternatives (resistance

heating) for achieving higher temperatures because they avoid the efficiency penalty associated with the thermal to electrical energy conversion while still enabling storage of thermal energy for later conversion to electricity if desired.

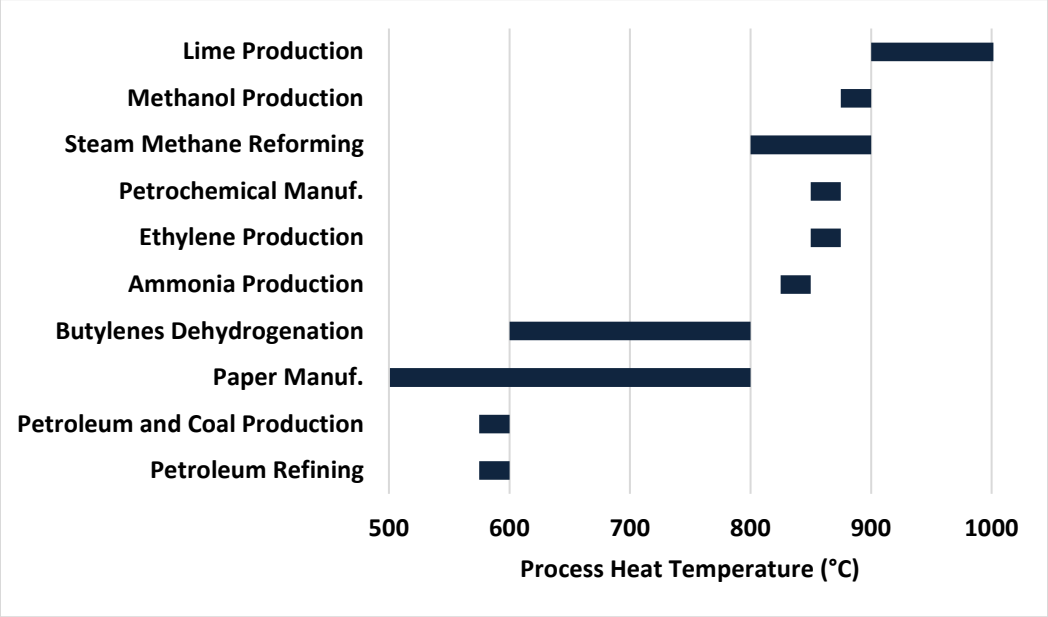

Figure 2. High-temperature industrial thermal processes with temperature requirements [7].

1.2 Chemical Heat Pump

Chemical Heat Pumps (ChHPs) utilize the reversible chemical reaction to change temperature levels of thermal energy (stored in chemical bonds of compounds) by manipulating reaction conditions. The advantages of ChHPs are their high-storage capacity, long-term storage of both reactant and product, lower heat loss, and energy upgrading for low-temperature heat [8]. Compared with mechanical and absorption heat pumps, ChHPs are capable of much higher temperature lifts with significantly less mechanical input [9]. A ChHP based on calcium hydroxide-oxide system is shown schematically in Figure 3. This system can also be operated as thermochemical energy storage system (TCES).

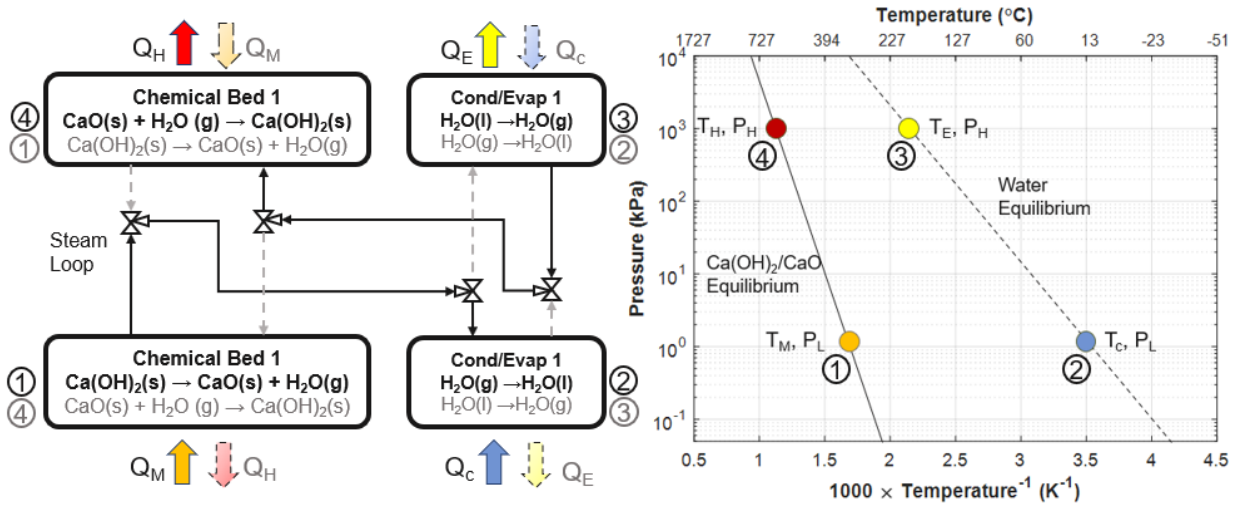

Figure 3. (a) Schematics of components of $Ca(OH)_2/CaO$ ChHP system; (b) Clausius-Clapeyron Diagram.

The attractiveness of $Ca(OH)_2$/CaO ChHP arises from the following points: (1) calcium hydroxide is relatively cheap and easily available, (2) the process has high storage density as reaction enthalpy is high, and (3) there is a wide range of operating temperatures (300–650°C) for the system [8]. Other common systems include processes based on thermal decomposition of ammonium salts or metal hydrides; sulfur dioxide, carbon dioxide, or hydrogen systems; and adsorption on a solid sorbent. However, these systems are more costly, involve species that are toxic in nature (such as NH_3 or SO_2, etc.), have issues related to reversibility, and the reagent handling is challenging, particularly when dealing with non-condensable gases.

The operation of this system can be described in two basic steps: charging and discharging, as shown in Figure 3. Charging starts with the addition of heat at T_M to dehydrate the chemical bed at low pressure. Then, the vapor is captured in a condenser and heat is rejected at T_C, usually the ambient temperature. For discharge, the vapor pressure is increased, and the water is evaporated with heat added at T_E. The vapor then hydrates the chemical bed, releasing the stored heat at T_H. Once the bed is done reacting, the bed can be charged again. The heat input and rejection temperatures of a chemical heat pump are mainly dictated by the saturation or equilibrium temperatures of the refrigerant or reactants used. In a survey conducted in 2013 by Sabharwall et al., the reversible $Ca(OH)_2$/CaO reaction shown in Equation 1 was established as the best candidate for high-temperature boosting of heat from light-water reactors to high-temperature industrial thermal processes [10].

$$CaO(s) + H_2O(g) \rightleftharpoons Ca(OH)_2 \quad (1)$$

The $Ca(OH)_2$/CaO reaction has a high-energy density, fast-reaction kinetics, and an equilibrium curve appropriate for the high temperatures involved with the industries of interest. A schematic of the $Ca(OH)_2$/CaO ChHP is shown in Figure 3a. The Clausius-Clapeyron diagram in Figure 3b shows the equilibrium curve for the reaction and the saturation curve of water. The calcium oxide hydration reaction has the potential to receive heat at 350°C during charging and deliver heat above 600°C during discharge. This means the reaction is not only helpful in delivering heat at high temperatures, but also temperature lifts greater than 250°C. High-temperature operation and large temperature lifts make the CaO/$Ca(OH)_2$ chemical heat pump a great candidate for efficient high-temperature process heating using low-carbon thermal energy.

Several researchers have investigated the $Ca(OH)_2$/CaO reversible system both theoretically and experimentally. Schaube [11] and Matsuda [12] used thermogravimetric analysis with 10–30 mg of $Ca(OH)_2$ for investigation of dehydration-hydration reversible reaction of $Ca(OH)_2$/CaO. Dai et al. [13] conducted dehydration and hydration on a small scale with powdered 20 g of $Ca(OH)_2$, and the gross heat input and outflow were calculated under standard conditions. Schmidt et al. [14] used a significantly bigger system containing 2.4-kg $Ca(OH)_2$ at a low pressure to test heat transfer fluids under varied heating and cooling loads. Schmidt et al. [15] designed chemical reactor indirectly operated by integrating heat exchanger at high temperature for 20-kg $Ca(OH)_2$ and Criado et al. [16] examined the reaction behavior in a fluidized bed system. Schaube et al. [17] studied the direct heat transfer output of CaO/$Ca(OH)_2$ in a fixed bed reactor containing 60-g powdered $Ca(OH)_2$. Funayama et al. [18] used 60 g of calcium hydroxide pellets to enhance the temperature of the $Ca(OH)_2$/CaO dehydration-hydration cycle, and the heat storage density of the bed was calculated assuming constant reaction enthalpy. The influence of temperature dependence on thermodynamic characteristics and reaction equilibrium was investigated by Gupta et al. [19] theoretically and temperature amplification was observed experimentally in a 300-g packed bed reactor [20]. Most of the above studies focused on the thermochemical energy storage aspect of $Ca(OH)_2$/CaO reaction system.

Modifying the reactant to improve its mechanical and physical properties has been the topic of a few recent investigations as studies have found an agglomeration of reactant giving rise to low effective thermal conductivity and poor heat and mass transfer. Criado et al. [21] studied the crushing strength and mechanical stability of a CaO-based material with $Na_2Si_3O_7$ as a modifier and discovered that decreasing the reaction time was a viable alternative for increasing the reactants' mechanical stability. For incomplete conversion of CaO to $Ca(OH)_2$, the crushing strength of CaO-based material particles was increased, but higher conversion resulted in a lower crushing strength. Yan et al. [22] looked at modifying a CaO-based material with LiOH to improve dehydration performance, but the modification had no effect on the solid reactant's structural integrity. Sakellarious et al. [23] added aluminum to CaO in the form of aluminum oxide, which improved structural stability while reduced the material's hydration activity. Adding a minimal amount of nano-SiO_2 to CaO particles prevented agglomeration and stabilized the bulk characteristics of CaO particles, but had little effect on lowering the dehydration temperature, according to Roßkopf et al. [24, 25]. Gupta et al. [26] investigated the effect of addition of $CaTiO_3$ with $Ca(OH)_2$ pellets and the results showed increase in rate of reaction with 55% increase in mechanical strength of the pellet.

1.3 SMR and ChHP Economics

The development of an SMR involves significantly less upfront money, resulting in lower financial risks and making it a viable alternative to large nuclear reactors (1 GW). SMR can also combine with a hybrid energy system to manage fluctuations in intermittent renewable energy generation while also storing energy or providing electricity/heat. Bolden et al. [27, 28] examined the SMR economics through a comprehensive model based on first-of -a-kind (FOAK) through nth-of-a-kind (NOAK). The model evaluates a project's feasibility in regards of market conditions and commonly used capital budgeting techniques like the net present value (NPV), internal rate of return (IRR), payback period (PBP), and the levelized cost of energy (LCOE). Sabharwall et al. [29] conducted a study on nuclear-renewable energy integration economics where study compares economic of three cases, i.e. nuclear, nuclear-wind and nuclear-wind-hydrogen for the PJM and Mid-C U.S. markets. Alonso et al. [30] conducted economic comparative study on SMR versus coal and combined cycle plants. They performed sensitivity analysis showing how NPV and IRR vary with changing discount rates and overnight capital cost. Within IES, there is an obvious requirement to resolve temperature mismatches between energy sources and demands in the most effective way feasible. The techno-economics model is critical for determining whether technical and market factors make the heat pump advantageous and appealing to investors.

Very few studies have focused on the economic feasibility of ChHPs because of low technology readiness level of the system. Spoelstra et al. [31] studied the techno-economic analysis of two different ChHPs for temperature amplification less than 150°C. The isopropanol-acetone and ammonia-salt systems were proposed. The ammonia-salt vapor heat pump outperforms the isopropanol-acetone heat pump in terms of technical performance by evaluating internal rate of return of 7%, as it has a higher enthalpic efficiency, a higher coefficient of performance, and does not produce by-products. Karaca et al. [32] investigated economics of ChHP based on ethanol–formaldehyde–hydrogen, ethanol–acetaldehyde–hydrogen, iso-propanol–acetone–hydrogen and n-butanol–butyraldehyde–hydrogen systems for low-temperature heat upgrade from 77–200°C. These studies were conducted in 2002, and the economy and policy have changed significantly since then. Bayon et al. [33] explored the techno-economic feasibility of thermochemical energy storage systems when coupled with solar thermal energy. The working pair investigated were molten salts, alkaline-hydroxides, carbonates, and oxides. Of 17 working pairs analyzed, eight showed high potential for commercial applications with a cost lower than \$25 MJ^{-1} including $Ca(OH)_2$/CaO system. There have not been any techno-economic studies reported which focuses on ChHP for thermo-amplification to boost the temperature from 350°C to 600°C and above.

2. RESEARCH OBJECTIVE

The two main objective of this study are: the pilot-scale study for 25-,100, and 1000- kW ChHP and techno-economic analysis of a coupled SMR-ChHP system.

2.1 Scale-up Study

The study focuses on the preliminary designing the ChHP pilot-scale setup for three different scales (e.g., 25-,100-, and 1000-kW system). Two input and output temperatures were assumed, and the heat transfer area was calculated for indirect heat transfer in the form of shell and tube reactor configuration. Based on the area estimated, cost of the chemical bed will be evaluated, and the schematic of the pilot-scale ChHP system will be designed.

2.2 Techno-economic Analysis

We also know that the ChHP system is better for the environment than using fossil fuels for process heating. The next step is to assess the economics to decide whether the system is a viable investment. The aim of this research is to study the economic feasibility of ChHPs when coupled with advanced SMR to deliver the heat for high-temperature thermal industrial processes. This study focuses on economic feasibility of SMR by selling electricity and nuclear hybrid energy system (NHES) (i.e., SMR coupled with the ChHP system) by selling heat and electricity combined. For techno-economic analysis, the average selling price of electricity and natural gas (for heat) for six different U.S regions will be used. The ChHP-specific capital cost was calculated using steady state thermodynamic model as there are no studies presently available which reported the specific cost of $Ca(OH)_2/CaO$ ChHP. The economic viability was compared by estimating the economic parameters such as NPV, payback period (PBP), discounted cash flow return (DCFR), and LCOE for SMR and NHES systems.

3. SCALABILITY STUDY OF CHEMICAL HEAT PUMP

Temperature amplification applications of ChHP coupled with nuclear reactor have not been investigated or published at pilot scale in the literature. Furthermore, the coupling of ChHP using different reaction system provides a compelling alternative for achieving the temperature mismatch between nuclear reactor and heat required for industrial applications. The pilot-scale study will yield valuable information on Integrated Nuclear Hybrid Energy Systems consisting of advanced reactors coupled to ChHP, which will be useful in defining the role of the nuclear energy in future energy systems. Research at the University of Idaho has successfully demonstrated the feasibility of the multiple cycles of $Ca(OH)_2/CaO$ ChHP. Results from the bench-scale experiments will be used for detailed design of pilot-scale setup, which will accurately model the full-scale process. Current challenges will be addressed that include poor heat transfer inside the chemical bed, mitigating any performance degradation by addition of inert in solid reactant, and measuring the flow rate of water vapor accurately as it is much easier to measure the flow in pilot scale, as compared with bench scale because of low volume of reactant, which will give us a better understanding of kinetics of the reaction. Experimental and theoretical results at pilot scale will yield valuable information for commercial scale Integrated Nuclear Hybrid Energy Systems, thus supporting missions in enhancing the energy security, and increase the role of nuclear energy in nation's energy system.

3.1 Literature Review of Pilot-Scale Study

Few studies have been conducted for thermochemical energy storage aspect of the $Ca(OH)_2/CaO$ reaction but not specifically for chemical heat pump by delivering the thermal heat in a continuous operation. Following are the studies focusing on the pilot-scale model for thermochemical energy storage.

3.1.1 10 kW Pilot-Scale Reactor

Schmidt et al. [15] focuses on hydration-dehydration cycles of indirectly operated reactor in pilot scale (20 kg of powdered CaO, particle size d_{50} = 5µm). The heat transfer fluid (HTF) used was air and HTF was heated up to 700°C via electric heaters. The specifications of the reactor are mentioned in Table 1.

Table 1. Specifications of the reactor.

Material (Reactor and Thermoshelves)	1.4404 – X2CrNiMo 17-12-2
Metal weight	145 kg
Reaction bed dimensions	45 L (≈25 kg powdered $Ca(OH)_2$) 20 × 200 × 800 mm (10 channels)
Max. permissible temperature	600°C
Max. permissible pressure	Reaction gas side: 0.1–2.5 bar HTF side: 0-5.0 bar
Thermoshelves dimensions	250 × 850 mm (10 channels) 4.25 m^2 total heat transfer area
Power	$P_{Nominal}$ = 5 kW P_{max} = 10 kW
HTF mass flow	0.00283-0.0531 kg/s
Operating conditions	Dehydration: Pressure = 10 kPa Temperature = 400–590°C Hydration: Pressure = 200 kPa Temperature = 550°C Total Cycles: 10

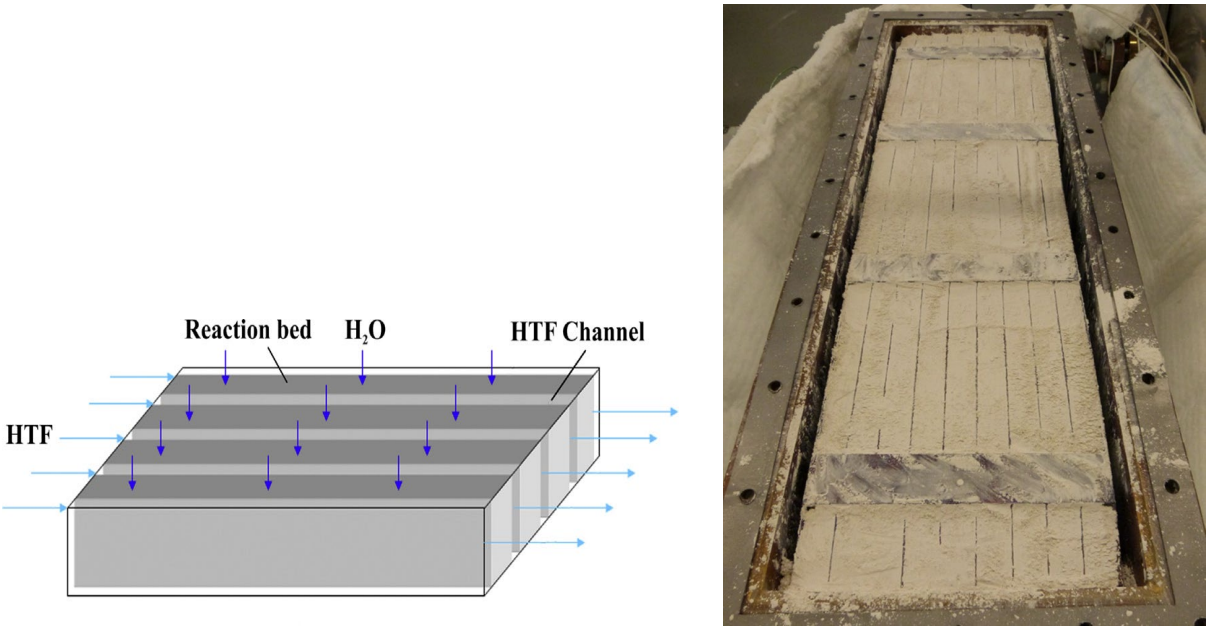

(a) (b)

Figure 4. (a) Schematic of the cross-flow diagram of the pilot reactor; (b) Reactor filled with 20 kg of $Ca(OH)_2$ [15].

The cross-flow arrangement between the HTF and the reaction gas allows for sufficient heat exchange area along the length of the reactor while the reaction gas only must overcome a short distance through the reaction bed to the bottom of the reactor, as shown in Figure 4a. The pressure drop over the reaction bed is minimal and a uniform equilibrium temperature over the entire bed volume can be expected. The reactor is filled with a mass of approximately 20 kg of $Ca(OH)_2$, as shown in Figure 4b.

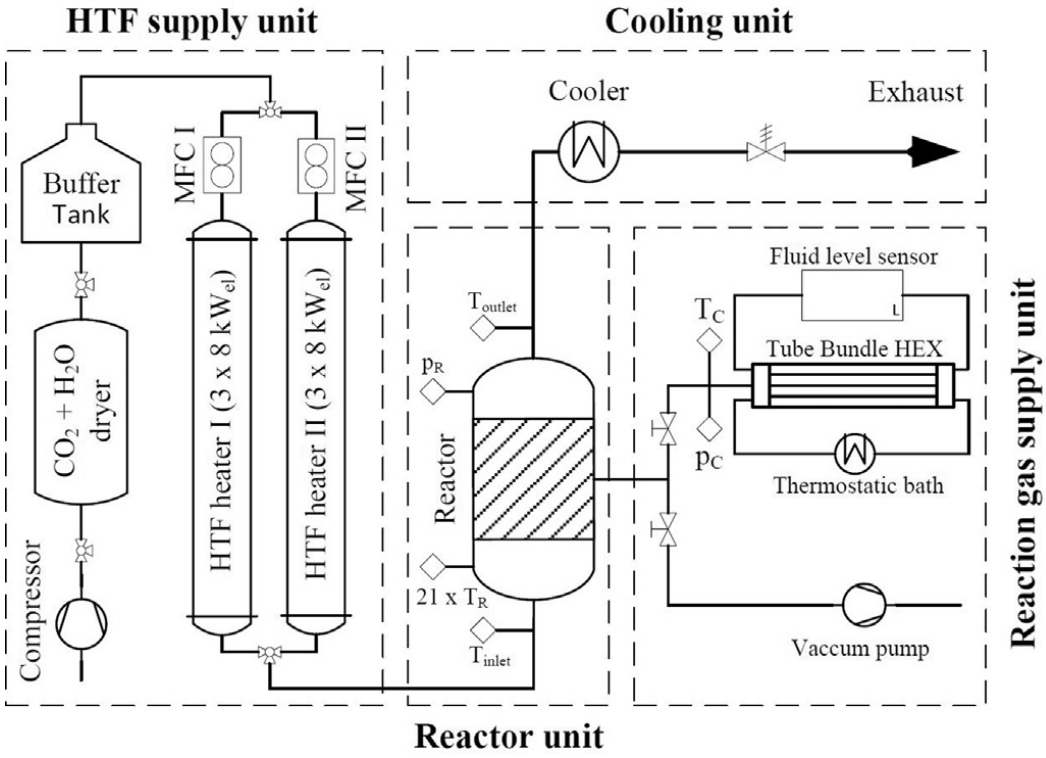

Figure 5. Process flow diagram of the test bench [15].

A compressor conveys ambient air with a maximum volume flow of 160 Nm^3/h at 10 bars. To ensure a continuous availability of the air flow a buffer tank is installed with a capacity of 1 m^3 air and a maximum pressure of 10 bars. The HTF flow can be adjusted in a range of 8 to 160 Nm^3/h via two mass flow controllers (Bronkhorst, digital flow controller, ±0.5%) at a pressure of up to 5 bar.

For the reaction gas supply an additional evaporator/condenser unit, shown in Figure 5, was developed. A tube-bundle heat exchanger with a casing volume of 8.5 l is filled with 2 l of distilled water. A vacuum pump is connected to evacuate the system down to an absolute pressure of 10 mbar to enable a pure water vapor atmosphere. The water level is constantly measured by a fluid level sensor (Vegaflex 65, coaxial measuring probe, ±2 mm).

Similar study was presented by Linder et al. [34], as shown in Figure 6, which showed the good agreement between the experimental and simulated results that the reaction kinetics determined in micro-scale measurements as well as the known bed properties offer a sufficient representation of the effective conditions within the bed.

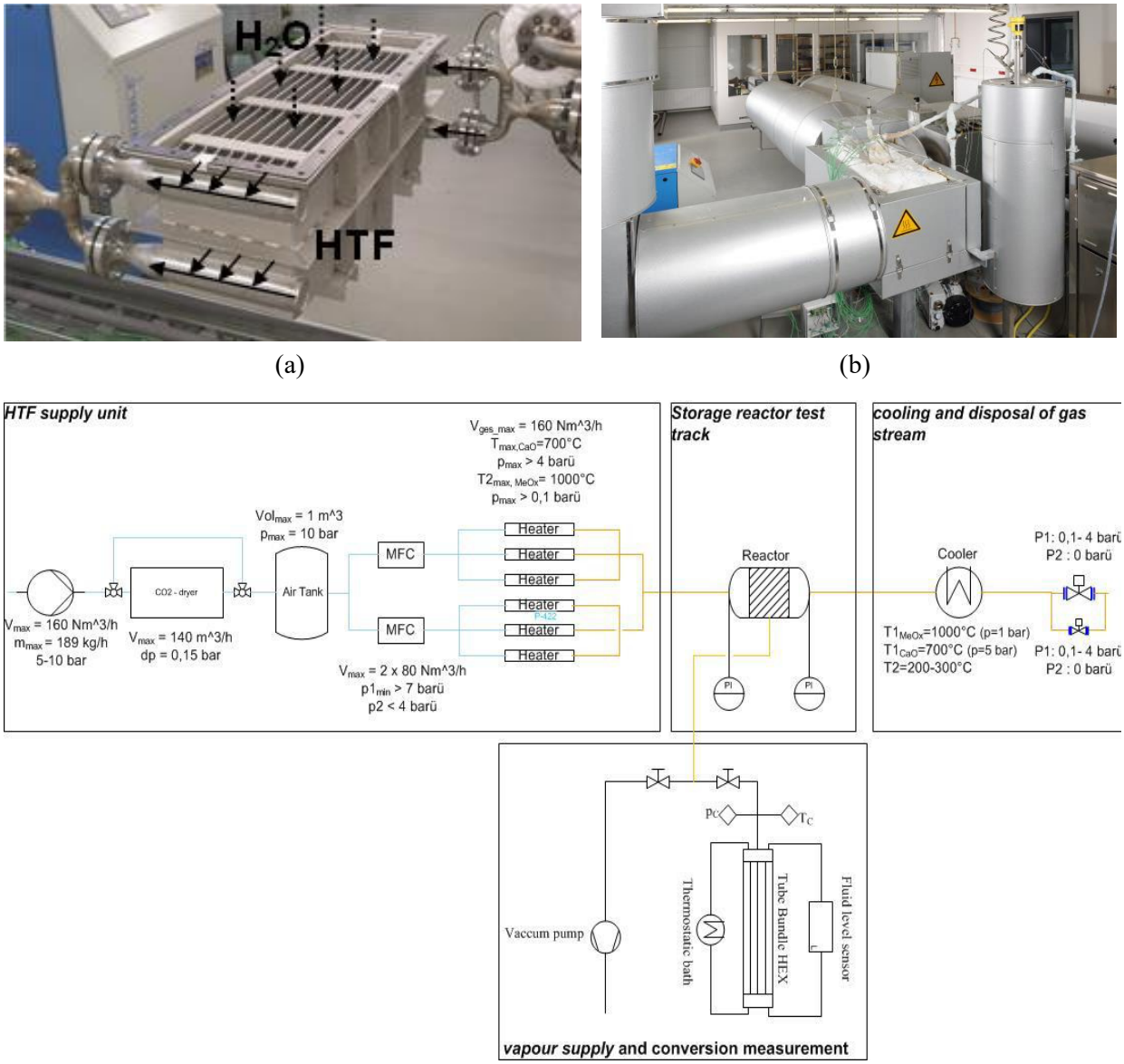

Figure 6. (a) Indirectly operated thermochemical storage reactor; (b) multifunctional test bench; (c) process flow diagram of the test bench with integrated indirectly operated reactor [34].

3.1.2 Design of MW-Scale Thermochemical Energy Storage Reactor

Angerer et al. [35] presented a theoretical study on a novel technical design of a MW-scale thermochemical energy storage reactor for CaO system. The reactor concept features a bubbling fluidized bed with a continuous, guided solid flow and immersed heat exchanger tubes. To investigate the reactor design, a model is build using clustered CSTRs. A fluidized bed reactor (FBR) was chosen in this work as the most promising reactor concept for large-scale application as shown in Figure 7.

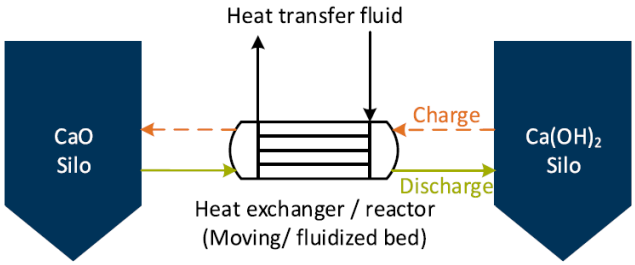

Figure 7. Schematic of a thermochemical storage system with separation of power (heat exchanger/reactor) and capacity (silos) [35].

The concept of the design of the reactor is shown in Figure 8. The FBR is operated as a dense bubbling bed. A special gas distributor plate with a high number of nozzles is used to distribute the fluidization gas uniformly over the reactor cross section. To improve the residence time distribution, baffles are integrated in the bed leading to a guided flow of solids (powdered reactant) from inlet to outlet.

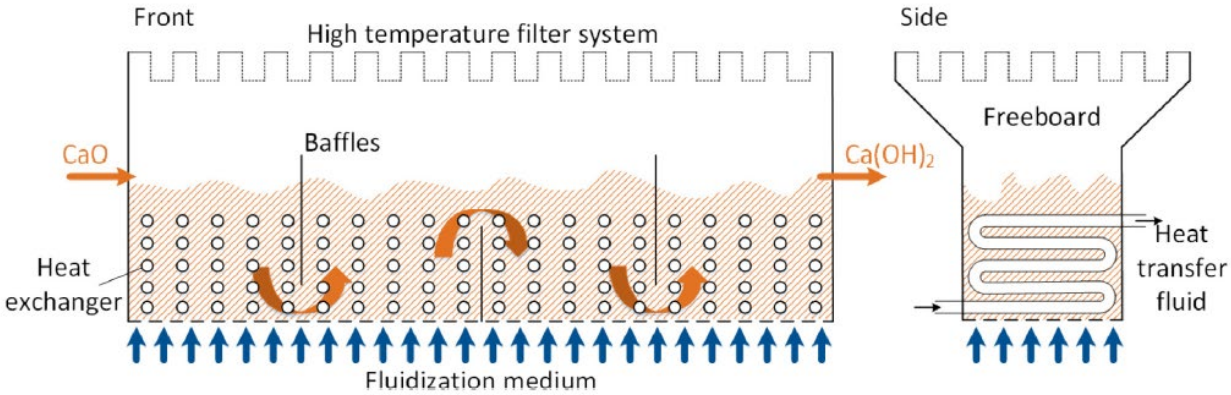

Figure 8. Reactor design of a continuous MW-scale FBR for thermochemical energy storage [35].

3.1.3 Moving Bed Pilot Plant for TCES CaO/Ca(OH)$_2$

In this work Schmidt et al. [36] investigated an indirectly heated moving bed concept realized in 10 kW/100 kWh scale. Figure 9a shows the basic design of the heat exchanger. The storage material flows in 158 tubes with an inner diameter of 28 mm. On the shell side of the heat exchanger the HTF air flows in counter-current direction. It enters the reactor at the connection at the right side and flows around the tubes directed by six baffle plates. The outlet of the HTF leaves the reactor at the opposite side. With an overall heat transfer area of 5 m² the heat exchanger is designed to transfer a power of 10 kW at a nominal airflow of 160 Nm³/h and a temperature difference between air inlet and outlet of 200 K.

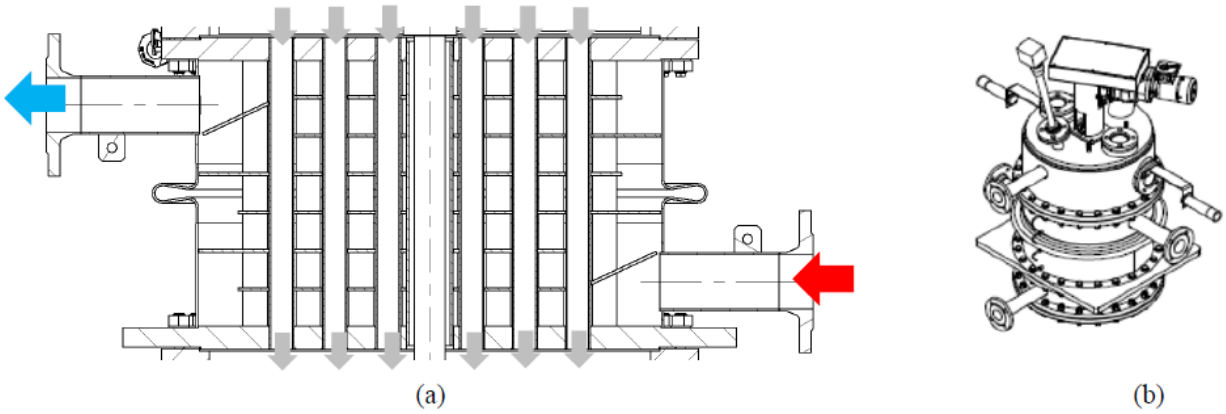

Figure 9. (a) Heat exchanger design for moving particles and air; (b) complete reactor design [36].

Figure 9b shows the complete reactor consisting of three attachable parts. First part is the top of the reactor where the material inlet is located. In the top is also an additional flange connection where the reaction gas can enter the reactor above the tube bundle. The middle part of the reactor is the heat exchanger. In the bottom of the heat exchanger the outlet area of the reactor is attached. In this part an additional connection is foreseen to supply or remove reaction gas from below the tube bundle. In the flat bottom area, a rotating scraper is installed to move material from the outer tubes to the outlet cross section located in the center.

Figure 10 shows the design of the moving bed pilot plant including transport and storage facilities for the material. In the first storage container approximately 270 kg of powdered $Ca(OH)_2$ material can be stored.

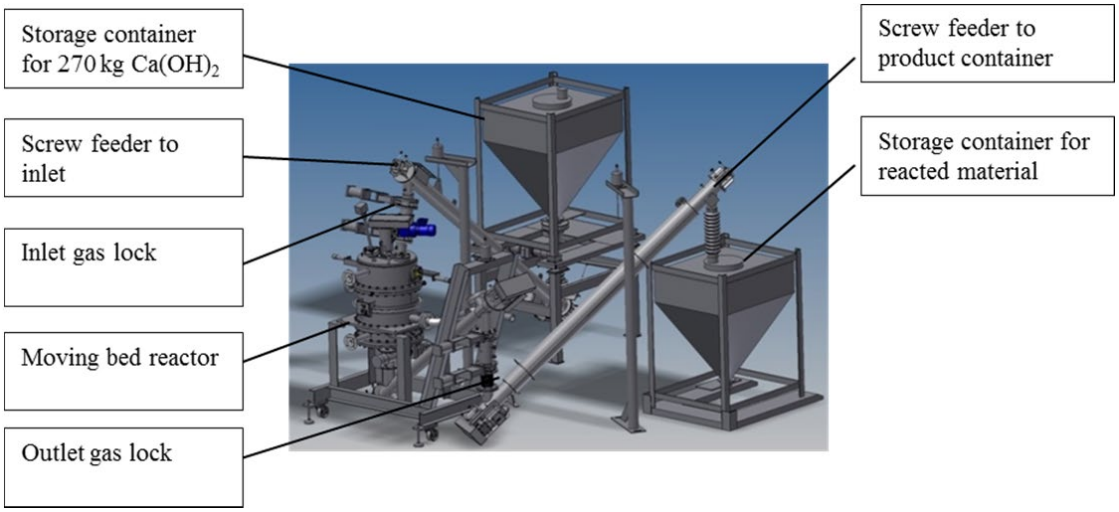

Figure 10. Reactor design of a continuous MW-scale FBR for thermochemical energy storage [36].

Figure 11 shows the integration of the pilot plant (yellow) into the existing test facility for thermochemical storage systems at DLR. The moving bed reactor is connected to the heat supply unit (green), which can deliver an air flow of 160 Nm^3/h at temperatures up to 1000°C. Additionally, the two reaction gas inlets of the reactor are connected to the condenser/evaporator unit (blue). With the condenser it is possible to adjust a water vapor atmosphere between 0.1 and 2 bar (10 and 200 kPa) in the reactor. The change of the water level in the condenser is measured giving the level of conversion in the reactor and ten cycles were studied.

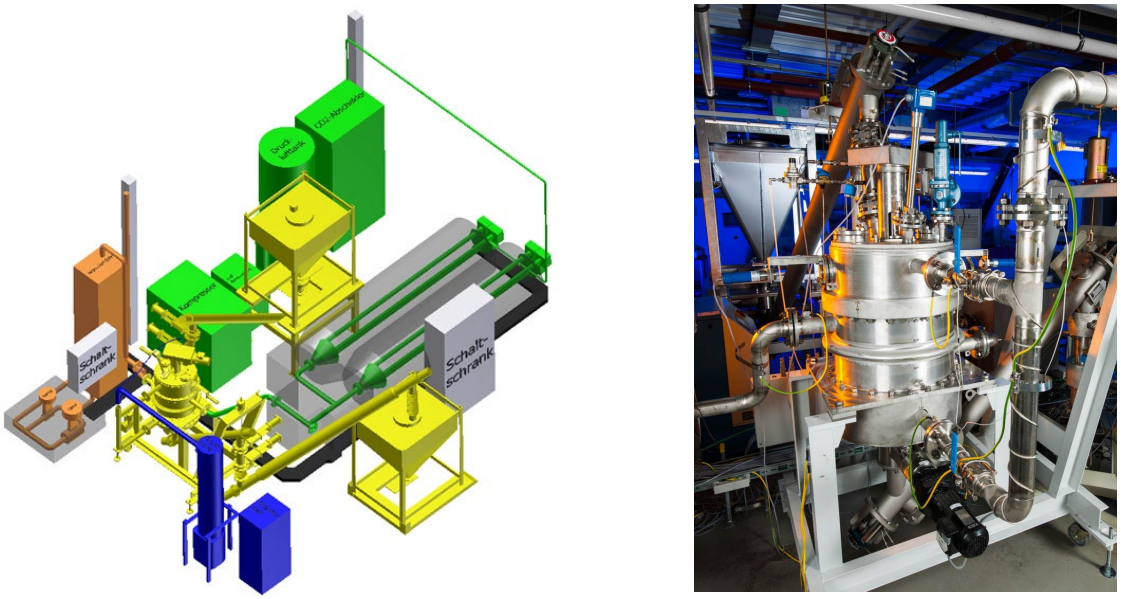

Figure 11. Integration scheme of the pilot plant into existing thermochemical test bench at DLR (German Aerospace Center) [36].

3.1.4 kW Moving Bed Reactor for TCES

A moving bed reactor for encapsulated storage materials in laboratory scale was developed and set into operation by Mejia et al. [37]. The reactor is designed to operate at pressures between 10 and 150 kPa and a maximum temperature of 550°C (key parameters are summarized in Table 2).

Table 2. Technical features of the moving bed reactor.

Heat exchanger type	Indirect, tube bundle
Tube diameter	18 mm
Tube length	330 mm
Number of tubes	22
Volume	1.85 l
Heat exchanger area	0.41 m^2
Thermal power	1 kW
Construction material	Stainless steel 1.4571
Operating Conditions	Dehydration: Pressure = 10 kPa Temperature = 540°C Hydration: Pressure = 100 kPa Temperature = 505°C Total Cycles: 6

The storage material flows inside the tubes, assisted only by gravity as shown in Figure 12. Thermal energy is delivered or taken up by the HTF, which flows on the shell side of the heat exchanger directed by baffle plates. These plates ensure a high velocity of the air flow to obtain a good heat transfer coefficient between the gas flow and the tube surface. The length of the tube defines the heat exchange area and the residence time of the reacting material in the tube. The granulated $Ca(OH)_2$ was used for experiments of diameters 1–4 mm.

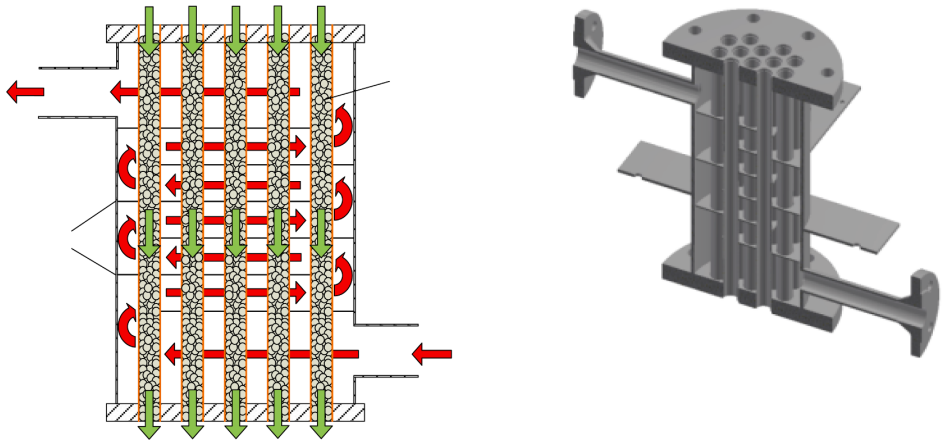

(a) (b)

Figure 12. (a) Schematic representation of the flow of the HTF and storage material; (b) 3D image of the tube-bundle reactor [37].

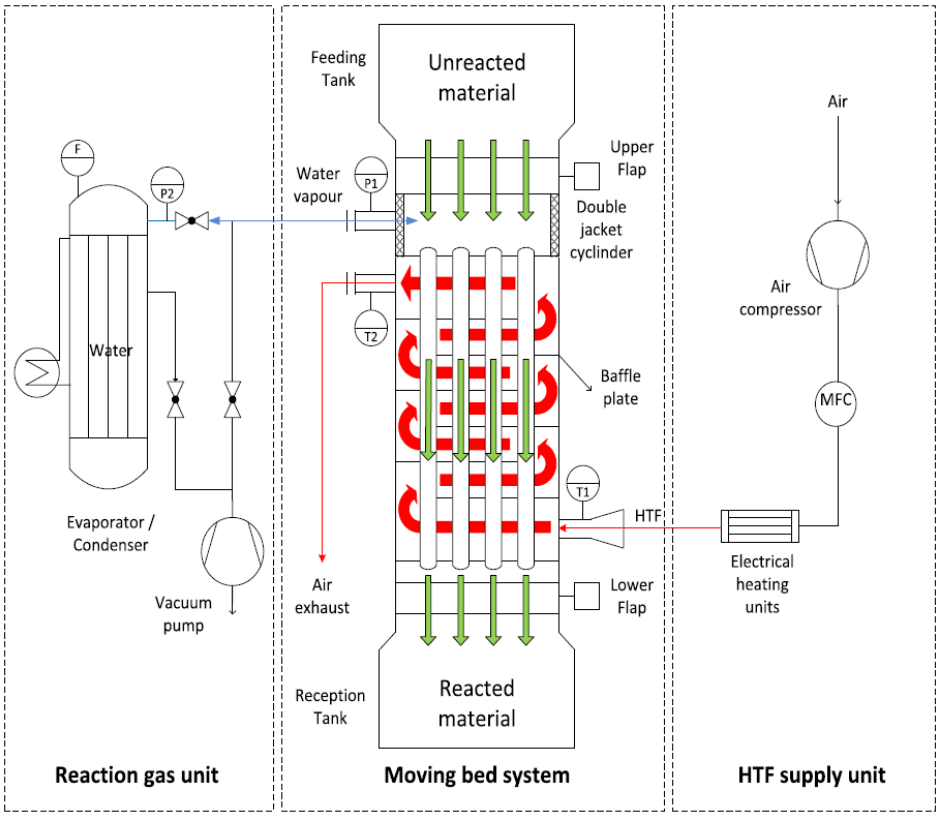

Figure 13. Schematics of the moving bed reactor integrated in the test bench [37].

The test bench consists of the moving bed system, the reaction gas unit, and the HTF supply unit as shown in Figure 13. Once all the tubes are filled with material, the hydration/dehydration process can start. As soon as the material in the lower part of the tube bundle has reacted completely, the lower flap is opened to allow the material to flow down to the reception tank. By controlling the mass flow in and out of the reactor, the system can be operated as a continuous moving bed, quasi continuous moving bed, or fixed bed, allowing the investigation of such operation modes. The reaction gas unit is composed by the evaporator/condenser, which is equipped with a filling level measurement sensor (Vegaflex 65,±2mm). The evaporator/condenser supplies water vapor at different pressures and depending on the direction of the reaction occurring in the reactor, the vapor is either taken up or released from the storage material. This causes a pressure change in the system, followed by compensation through further evaporation or condensation of water in the reaction gas unit.

All the studies focused on the indirect heat transfer to transfer heat to/from chemical bed through heat exchangers via HTF. The studies focused on three types of reactors (i.e., fixed bed, moving bed, and fluidized bed reactors).

- Due to the low-thermal conductivity of the $Ca(OH)_2$ material large storage capacities operated in an indirectly heated fixed bed also require large heat exchangers. On approach was to detach the costly reactor with the heat exchanger (power) from the storage material (capacity) and this can be accomplished by a moving bed concept where the material moves through the reactor.
- In moving bed, the volume of the granules also expanded during the hydration procedure causing clogging in the heat exchanger tubes in the presented reactor. Thus, a free flow of the granules through the reactor after hydration was not achieved yet.
- The fluidized bed concept showed promising MW-scale TCES system claiming that reaction is limited by heat transfer and further research is necessary to identify ideal fluidization conditions to maximize heat transfer while minimizing parasitic losses and improve the storage materials cycling stability and physical properties required for fluidization.

3.2 Pilot Plant Theory

A pilot plant is the tool intended to allow investigation of a process or a process problem on a manageable scale in a realistic manner in a timely fashion. The pilot plant work is undertaken for a variety of goals. Some of the most common are: (1) determining process economics, (2) performing process development, (3) demonstrating technical feasibility, (4) providing technical services and, (5) supporting market development. Based on size, the pilot plants are classified as laboratory-scale, benchtop pilot plants or microunits; integrated pilot plants or research-scale pilot plants; and demonstration units, semiworks units, or prototype units as shown in Table 3.

Table 3. Typical size classification of pilot plants.

Classification	Synonyms	Typical Scale	Typical Material of Construction	Typical Volume of Materials	Typical Operating Pressure	Cost Range (Thousands of Dollars)
Laboratory-scale pilot plants	Benchtop units Laboratory units Microunits	Small 1/16-1/4 in tubing 0.5–1.0 m^2	Glass Some metallic	Low Typically <1 L	Low to medium Typically <7000 kPa	$25–$100
Integrated pilot plants	Open-bay pilot plants	Medium to large	Metallic Some plastic	Medium to large Typically drums to	Medium Typically < 35,000 kPa	$50–$500

Classification	Synonyms	Typical Scale	Typical Material of Construction	Typical Volume of Materials	Typical Operating Pressure	Cost Range (Thousands of Dollars)
	Research-scale pilot plants Process simulations	½–2 in tubing or pipe 0.2–15 m^2		4000-L tanks		
Demonstration units	Semiworks units Prototype units	Large 1–8 in tubing or pipe ≥900 m^2	Metallic Some plastic	Large Typically 4000–40,000 L tanks	Medium Typically < 21,000 kPa	$500–$10,000

There are three basic methods for estimating the cost to design and construct a pilot plant: similarity, cost ratios, and detailed labor and material cost. *Similarity* involves estimating the cost of the pilot plant based on the costs of designing and constructing a similar unit. This approach can produce excellent results if the two units are almost identical, including the actual design, equipment, construction, and space. *Cost ratios* are used extensively in process plant estimation. They develop the cost estimate by relating the overall cost of the pilot plant or a part of the pilot plant to a known factor such as the cost of major process equipment, the number of control loops, the size of the equipment, or a variety of similar factors. *Detailed labor and material estimating* method involves breaking the pilot plant construction down into a detailed series of small tasks and estimating the labor and material required for each separate task.

Pilot plant activities can take place in a variety of spaces. To maximize pilot plant operations, it's critical to grasp the differences between them, as well as their benefits and drawbacks. Pilot plant space is often separated into four categories: (1) separate building, (2) containment cell, (3) open bays, and (4) hoods and laboratory areas. Pilot plant design is divided into two categories: (1) traditional design procedures that imitate commercial process processes, and (2) establishing a unique design tailored to the pilot plant. Safety in Pilot Plant Operations: Pilot plant operations are labor intensive and technically demanding activities. This increases the difficulty in ensuring a safe operation for a variety of reasons. While every organization has a slightly different safety review cycle, a list of the most typical ones is as follows. The preliminary or conceptual safety review is designed to identify potential problem areas before the design proceeds very far. The reappropriation or budget review is intended to ensure that sufficient funding is included for all major safety items in the budget. The preconstruction, design, or prebuild safety review is intended to review all aspects of the proposed pilot plant before construction begins. The preoperational or startup safety review is designed to concentrate on reviewing the actual proposed operations and examining the final construction product. The decommissioning or end-of-service safety review is intended to ensure that a unit is left in a safe condition when taken out of service.

3.3 Pilot-Scale Design

For the pilot-scale study, a two-bed system is considered where one will be dehydrating and other will be hydrating as shown in Figure 14. Once the one bed dehydrates completely will be switched to hydration reaction. The condenser will condense the water vapor coming out during the dehydration reaction. While the evaporator will produce high-pressure steam for hydration process. Both evaporator and condenser will have a mass flow controller to monitor the mass change in the chemical bed to study the kinetics of the reaction. The chemical beds will have several thermocouples and pressure gauges to monitor the temperature and pressure during the reactions, respectively. A storage tank to store the HTF will be connected to a pump. Heaters will be used to heat the HTF. Vacuum pump will be used to ensure there is no trace of impurity within the system and help maintain the sub-atmospheric pressure as well. Cooler will be used to cool down the HTF before storing it in the storage tank. Several temperature readers and pressure gauges will be used to monitor the parameters of interest through the process.

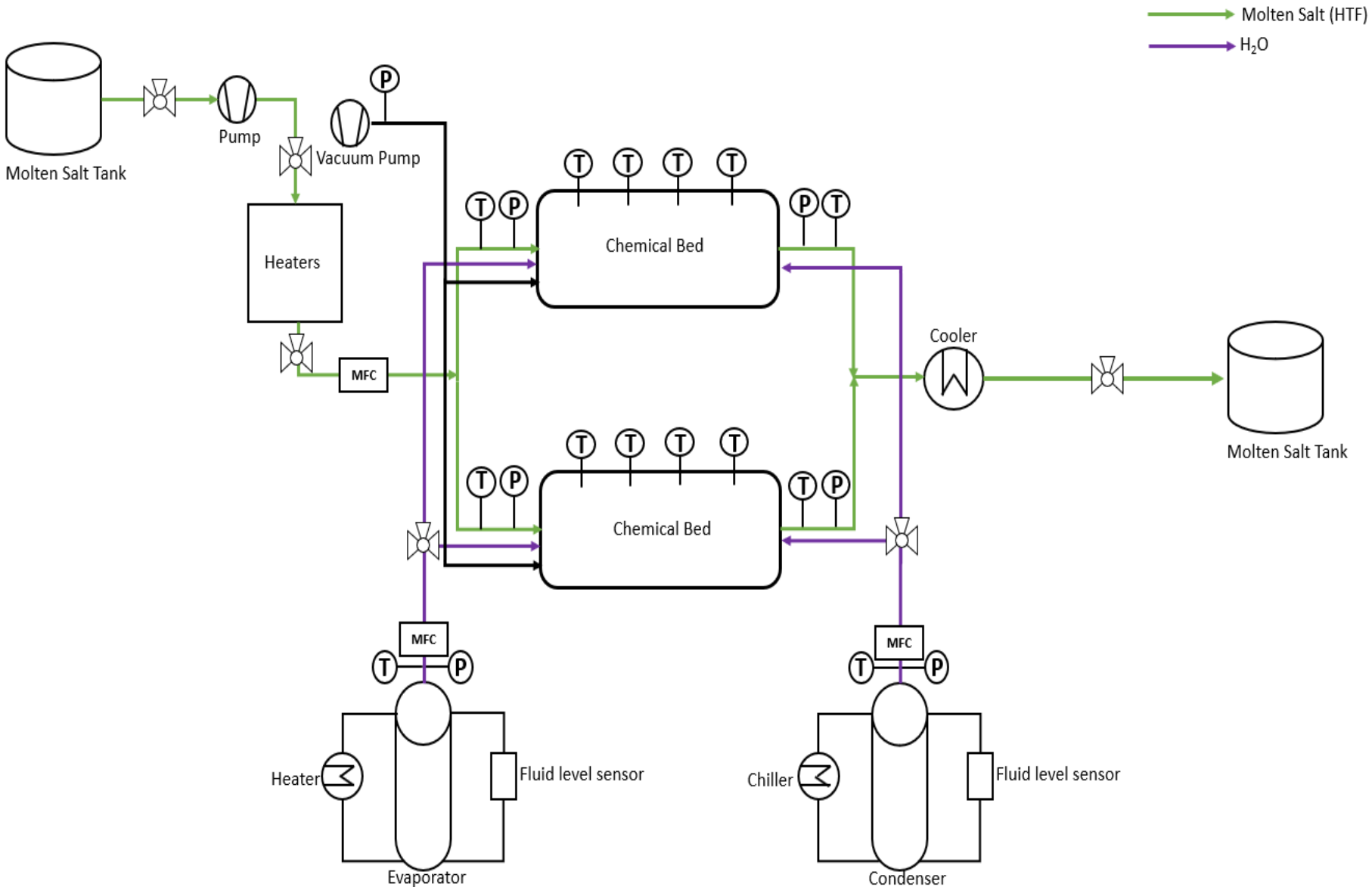

Figure 14. Schematics of the pilot-scale ChHP system with two chemical beds.

3.4 Thermal Calculations

For the capital cost of $Ca(OH)_2$/CaO ChHP, there are no estimates available in literature. A fundamental bottom-up approach for estimation of capital cost is built on based on the chemical bed cost using steady-state thermal model and other facility assumptions. The chemical beds are projected to be the biggest and most costly components in the ChHP system, based on our earlier work by Armatis et al. [38]. To acquire some technical and economic estimates for a big chemical bed design, a quotation from CG Thermal [39] was provided because chemical bed is not effectively represented by heat exchangers or chemical reactor cost curves. The specific cost of chemical bed based on heat transfer is assumed to be ranging from \$400 to \$600/ft^2 as per quotation from CG Thermal [39]. To estimate the specific cost of chemical bed, heat transfer area is estimated by the approach used in our previous work [38]. The system of six unknowns (L_{tube}, A_{HT}, U_{de}, U_{hy}, $\dot{Q}_{de}$, and ΔT_{hy}) are calculated by six equations mentioned in Equations 2–7. Once the heat transfer area is obtained, the chemical cost of the chemical bed can be estimated. The chemical bed volume V_{bed} is known for the given system size by using the approach from Armatis et al. by knowing the total number of moles and density of the reactant. The $\dot{Q}_{hy}$ is assumed based on the thermal output of the ChHP. ΔT_{de} and ΔT_{hy} are defined as the minimal difference between the average CaO/$Ca(OH)_2$ temperature and the molten salt temperature during dehydration and hydration. The dehydration temperature difference is assumed to be 15.5°C. The bed dimensions are calculated based on the nominal specifications provided by CG Thermal i.e., D_{shell} = 2.9 m, OD_{tube} = 25.4mm, ID_{tube} = 19.1 mm and n_{tubes} ranges from 10 to 550 based on the size of the system.

$$V_{bed} = \left(\frac{\pi}{4}\right)[(OD_{tube} + 2t_{bed})^2 - OD^2{}_{tube}]n_{tubes}L_{tube} \tag{2}$$

$$U_{de} = \left[\left(\frac{t_{bed}}{k_{bed}}\right) + R_c + \left(\frac{1}{h_{c,de}}\right)\right]^{-1} \tag{3}$$

$$U_{hy} = \left[\left(\frac{t_{bed}}{k_{bed}}\right) + R_c + \left(\frac{1}{h_{c,hy}}\right)\right]^{-1} \tag{4}$$

$$\dot{Q}_{de} = U_{de}A_{HT}\Delta T_{de} \tag{5}$$

$$\dot{Q}_{hy} = U_{hy}A_{HT}\Delta T_{hy} \tag{6}$$

$$A_{HT} = \pi OD_{tube}n_{tubes}L_{tube} \tag{7}$$

The schematic of the cross section of a single shell and tube heat exchanger design with chemical bed is shown in Figure 15. The reactant comprising of $Ca(OH)_2$/CaO is assumed to be layered around the tube outside in shell section. Most of the volume in shell side will be utilized by the water vapor during dehydration-hydration reactions.

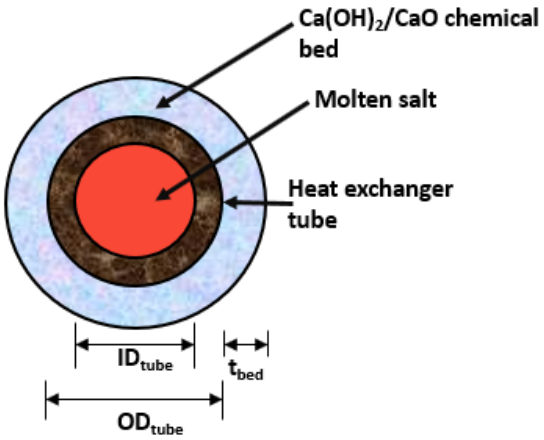

Figure 15. Cross-section view of single tube inside.

The molten salt convective heat transfer resistance, the CaO/Ca(OH)$_2$ contact resistance, and the CaO/Ca(OH)$_2$ conduction resistance are used to estimate the overall heat transfer coefficients for dehydration and hydration reaction. The Dittus-Boelter correlations are used to compute the dehydration and hydration convective heat transfer as shown in Equation 8–12. The heat transport from the reaction steam in the bed via convection and radiation, as well as tube conduction resistance, is assumed negligible. The mass and energy balances of the chemical beds from the system model given above are used to calculate the volume flow rate of the molten salt V_f. The Nusselt number for dehydration is calculated using Equation 11 and for hydration using Equation 12. The thermal conductivity of the Ca(OH)$_2$/CaO is evaluated between the range of 0.1 to 0.55 W/mK [14] and for this study it is assumed to be 0.5 W/mK. Based on Linder et al. [34] work, the contact resistance R_c is assumed to be 0.147 m^{2}K/kW.

$$h_c = \frac{Nu.k_f}{ID_{tube}} \tag{8}$$

$$Re = \frac{\rho_f ID_{tube} u_b}{\mu_f} \tag{9}$$

$$u_f = \frac{\dot{V}_f}{(\frac{\pi}{4}) ID_{tube}{}^2 n_{tubes}} \tag{10}$$

$$Nu = 0.0265 Re^{4/5} Pr^{0.3} \tag{11}$$

$$Nu = 0.0243 Re^{4/5} Pr^{0.4} \tag{12}$$

$$cost_{bed} = A_{HT} n_{bed} bed_{s,cost} \tag{13}$$

After solving for heat transfer area required for a single bed, the total capital cost of the ChHP chemical bed can be calculated by using the Equation 13, where n_{bed} is number of total chemical bed and $bed_{s,cost}$ specific cost of bed based on heat transfer area ($/m^2), which is assumed to be $4,305 $/m^2 CG Thermal [39]. Based on the thermal model, the heat transfer areas are calculated for three different scales (25-, 100-, and 1000-kW) and two different output temperatures (650 and 700°C), which are listed in Table 4. The input temperature of ChHP plays an important role and two input temperatures were considered for this study (425 and 450°C). The area required for 425°C is almost double compared with at 450°C because of slow reaction kinetics of $Ca(OH)_2$/CaO system at 425°C.

For pilot-scale study, the main contributor to the capital cost of the ChHP is the chemical beds. ChHP capital cost is assumed to be 90% of the total purchased cost of the equipment and other cost includes condenser, evaporator, and pump cost with is assumed to be within the 10% of the total purchased cost. The purchase price of the equipment is only a percentage of the entire investment and other costs are involved in the construction of a facility, which are summarized in Table 5. The total capital investment can be calculated using cost estimates for acquired equipment and expected proportions for each category. Based on Perter et al. [40] total capital investments were modified for ChHP system and were adjusted for the total sum to be 100%.

Table 4. Pilot-scale process parameters.

Heat Transf. Fluid Temp.		Bed Temp.									
Dehydration	Hydration	Dehydration	Hydration	Heat Output	Single Bed Heat Transfer Area	No. of Tubes	Length of Tubes	Bed Thickness	Cost of Chemical Bed (2 beds)	Other Equipment Cost (Condenser, Evaporator, Storage Tank, Heaters)	Total Equipment Cost
°C				kW	m^2	-	m	mm	$	$	$
425	650	377.5	674.39	1000	219.38	550	4.999	1.938	$1,901,389.99	$190,139.00	$2,091,528.99
425	700	377.5	724.26	1000	223.76	550	5.098	2.005	$1,939,351.92	$193,935.19	$2,133,287.11
450	650	395	680.79	1000	130.99	550	3.985	1.279	$1,135,304.38	$113,530.44	$1,248,834.82
450	700	395	730.48	1000	133.51	550	3.042	1.326	$1,157,145.49	$115,714.55	$1,272,860.04
425	650	380	672.38	100	21.27	40	6.664	1.735	$184,349.37	$61,449.79	$245,799.16
425	700	380	722.28	100	21.702	40	6.799	1.795	$188,093.56	$62,697.85	$250,791.42
450	650	397.5	678.9	100	12.586	40	3.943	1.174	$109,084.21	$36,361.40	$145,445.62
450	700	397.5	728.66	100	12.834	40	4.021	1.216	$111,233.65	$37,077.88	$148,311.54
425	650	380	672.38	25	5.317	10	6.644	1.73	$46,083.01	$15,361.00	$61,444.01
425	700	380	722.28	25	5.426	10	6.928	1.73	$47,027.72	$15,675.91	$62,703.63
450	650	397.5	678.9	25	3.146	10	3.943	1.174	$27,266.72	$9,088.91	$36,355.63
450	700	397.5	728.66	25	3.208	10	4.021	1.216	$27,804.08	$9,268.03	$37,072.11

Table 5. Total capital investment for ChHP pilot-scale system.

kW			25				100				1000			
Input Temperature (°C)			425		450		425		450		425		450	
Output Temperature (°C)			650	700	650	700	650	700	650	700	650	700	650	700
FCI %		FCI % adj												
50	Purchased Equipment	46.2963	$61,444.01	$62,703.63	$36,355.63	$37,072.11	$245,799.16	$250,791.42	$145,445.62	$148,311.54	$2,091,528.99	$2,133,287.11	$1,248,834.82	$1,272,860.04
10	Equipment Installation	9.259259	$12,288.80	$12,540.73	$7,271.13	$7,414.42	$49,159.83	$50,158.28	$29,089.12	$29,662.31	$418,305.80	$426,657.42	$249,766.96	$254,572.01
6	Instrumentation	5.555556	$7,373.28	$7,524.44	$4,362.68	$4,448.65	$29,495.90	$30,094.97	$17,453.47	$17,797.38	$250,983.48	$255,994.45	$149,860.18	$152,743.20
8	Piping	7.407407	$9,831.04	$10,032.58	$5,816.90	$5,931.54	$39,327.87	$40,126.63	$23,271.30	$23,729.85	$334,644.64	$341,325.94	$199,813.57	$203,657.61
3	Electrical	2.777778	$3,686.64	$3,762.22	$2,181.34	$2,224.33	$14,747.95	$15,047.48	$8,726.74	$8,898.69	$125,491.74	$127,997.23	$74,930.09	$76,371.60
2	Buildings	1.851852	$2,457.76	$2,508.15	$1,454.23	$1,482.88	$9,831.97	$10,031.66	$5,817.82	$5,932.46	$83,661.16	$85,331.48	$49,953.39	$50,914.40
2	Yard Improvements	1.851852	$2,457.76	$2,508.15	$1,454.23	$1,482.88	$9,831.97	$10,031.66	$5,817.82	$5,932.46	$83,661.16	$85,331.48	$49,953.39	$50,914.40
8	Service Facilities	7.407407	$9,831.04	$10,032.58	$5,816.90	$5,931.54	$39,327.87	$40,126.63	$23,271.30	$23,729.85	$334,644.64	$341,325.94	$199,813.57	$203,657.61
1	Land	0.925926	$1,228.88	$1,254.07	$727.11	$741.44	$4,915.98	$5,015.83	$2,908.91	$2,966.23	$41,830.58	$42,665.74	$24,976.70	$25,457.20
5	Engineering and Supervision	4.62963	$6,144.40	$6,270.36	$3,635.56	$3,707.21	$24,579.92	$25,079.14	$14,544.56	$14,831.15	$209,152.90	$213,328.71	$124,883.48	$127,286.00
5	Construction Expenses	4.62963	$6,144.40	$6,270.36	$3,635.56	$3,707.21	$24,579.92	$25,079.14	$14,544.56	$14,831.15	$209,152.90	$213,328.71	$124,883.48	$127,286.00
1	Legal Expenses	0.925926	$1,228.88	$1,254.07	$727.11	$741.44	$4,915.98	$5,015.83	$2,908.91	$2,966.23	$41,830.58	$42,665.74	$24,976.70	$25,457.20
2	Contractor's Fee	1.851852	$2,457.76	$2,508.15	$1,454.23	$1,482.88	$9,831.97	$10,031.66	$5,817.82	$5,932.46	$83,661.16	$85,331.48	$49,953.39	$50,914.40
5	Contingency	4.62963	$6,144.40	$6,270.36	$3,635.56	$3,707.21	$24,579.92	$25,079.14	$14,544.56	$14,831.15	$209,152.90	$213,328.71	$124,883.48	$127,286.00
108		100												
	Total FCI ($)		$132,719.07	$135,439.84	$78,528.15	$80,075.75	$530,926.19	$541,709.46	$314,162.53	$320,352.92	$4,517,702.61	$4,607,900.15	$2,697,483.20	$2,749,377.68

4. TECHNO-ECONOMIC ANALYSIS

Techno-economic Analysis (TEA) is a methodology framework utilized to analyze the technical and economic performance of a process, product, or service and "includes studies on the economic impact of research, development, demonstration, and deployment of technologies" quantifying the cost of manufacturing and market opportunities. TEA combines process modeling and engineering design with economic evaluation. It helps to assess the economic viability of a process and provides direction to research, development, investment, and policy making. To study the techno-economic feasibility of the system, the economic parameters are evaluated such as NPV, payback period (PBP), DCFR, and LCOE as described in the subsequent sections.

4.1 Methodology

The general methodology used to assess the techno-economic feasibility of a system is shown in Figure 16. The first stage is to estimate the capital costs of the system. In next step, possible market and utility factors are evaluated. Finally, the necessary economic parameters are calculated to determine the techno-economic feasibility of the system or project. This section will focus on the evaluation of economic parameters, specific capital cost, and baseline schematic of ChHP with SMR.

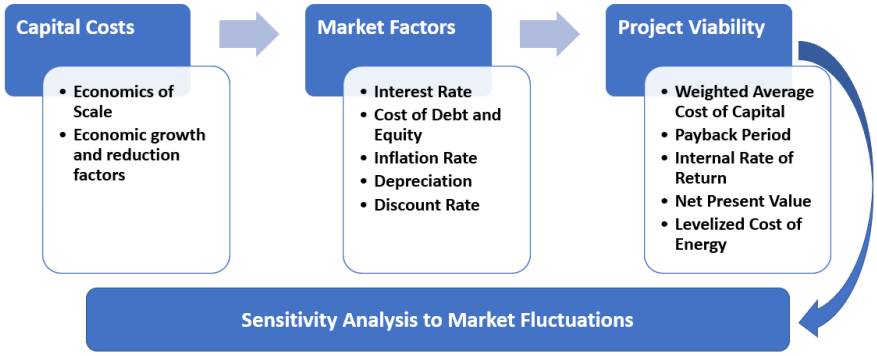

Figure 16. Overview of economic analysis methodology.

Once the capital costs are calculated for a particular SMR project, it is necessary to assess the market conditions and project viability. This is done by analyzing investment risks and determining the IRR, NPV, and LCOE for comparison to the weighted average cost of capital (WACC) and expected electricity prices.

4.1.1 Baseline ChHP Coupled SMR System

The schematic of the baseline model used in this study is shown in Figure 17 where ChHP is integrated with advanced SMR to deliver heat to high-temperature thermal industrial processes. This flow sheet shows the major components of the techno-economic model. The system uses thermal energy from the advanced SMR via molten salt as HTF and deliver it to chemical bed, which contains $Ca(OH)_2$ for dehydration process. In dehydration bed, $Ca(OH)_2$ decomposes into CaO in an endothermic reaction liberating water vapor. The molten salt returns from the dehydration bed and is reheated in a closed loop. The liberated water vapor from the dehydration bed is condensed in the condenser. At the same time a high-pressure steam from the evaporator is pumped to the Chemical Bed 2, which reacts with CaO to form $Ca(OH)_2$ in an exothermic reaction. This is a hydration step and the temperature in the hydration bed is higher than temperature in dehydration bed. According to Clausius-Clapeyron equilibrium relation, higher pressure dictates the higher temperature. The heat from the hydration bed is removed using molten salt, which is sent to the high-temperature thermal industrial processes. This salt is again sent back to the hydration bed. This process is continuous; and once the bed is dehydrated, it is ready for hydration and vice-versa.

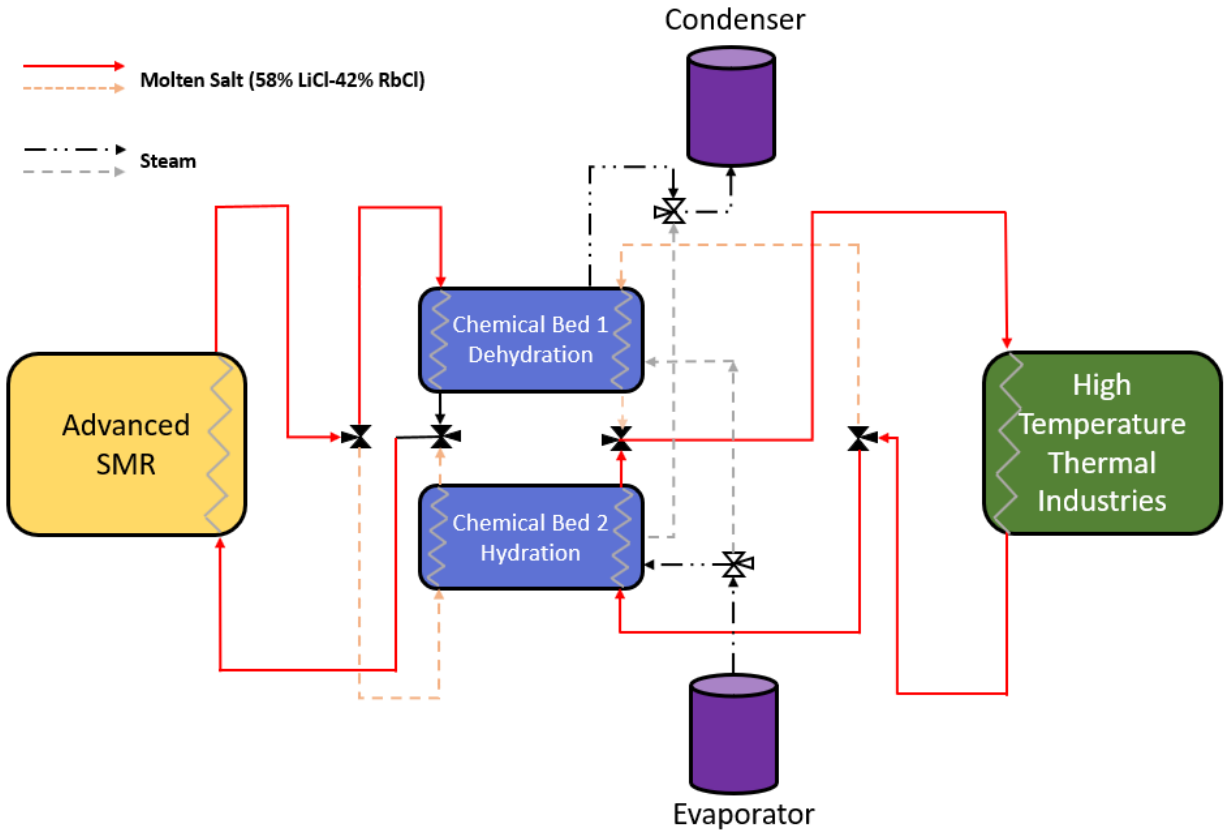

Figure 17. Schematic of ChHP coupled with SMR system.

The study focuses on advanced SMR with a thermal output of 100 MW_{th} is assumed and a temperature output of 400°C. The dehydration occurs at 380°C, and during hydration the molten salt temperature reaches to 650°C for this study. The conventional light water SMR operates at 300–325°C, making the reaction kinetics slow because of that reason dehydration temperature assumed in this study is slightly higher.

4.1.2 Assessment of Capital Cost of System

The estimation of advanced SMR cost and ChHP are both required for TEA of the system. Many studies have reported the capital cost of the advanced SMR. Sabharwall et al. [29] estimated the overnight capital cost (OCC) of SMR of \$4,637/kW_e. Richards et al. [41] estimated the overnight specific capital cost of the molten salt reactors between \$2,000 to \$3,846/kW_e. A study conducted by MIT [3] assessed the OCC for NOAK reactors between \$3,797 to \$6,880/kW_e based on a different design. FOAK SMRs OCCs were projected with 10th-of-a-Kind estimates in a recent report Stewart et al. [42]. FOAK SMRs can range in price from \$4,500 to \$8,500/kW_e depending on the reactor type. After ten reactors, the price range can be reduced to \$3,000 \$5,000/kW_e as per NOAK model. For this study, an OCC of will be \$4,637/kW_e assumed and a parametric study is also conducted assuming OCC ranging from \$4,500 to \$6,500/kW_e. According to Boldon [28], the total specific capital cost can be computed by integrating the contingency cost rate, detailed design, and engineering cost rate and the overnight capital cost, as shown in Equation 14. For this study, both the cost rates (contingency cost and detailed design and engineering) were assumed to be 5%.

$$TSCC = OCC(CC + DD\&E + 1) \quad (14)$$

4.1.3 Payback Period

The payback period (PBP) is the length of time required to recoup the funds expended in an investment, or to reach the break-even point and is calculated using the following Equations 15–17 where *PBP* is the payback period, *V* denotes the fixed capital investment, $\bar{A}$ denotes the average yearly cash flow over the project's lifetime, *A* is the annual cash flow or annuity, *N* denotes the project's length in years, *s* represents sales, c_0 represents cost, *d* represents depreciation, Φ represents the corporation tax rate, and *j* denotes a specific year [40].

$$PBP = \frac{V}{\bar{A}} \tag{15}$$

$$\bar{A} = \frac{1}{N}\sum_{j=1}^{N} A_j \tag{16}$$

$$A_j = \left(s_j - c_{o,j} - d_j\right)(1 - \Phi) + d_j \tag{17}$$

Compounding and discounting effects do not apply in this calculation since the payback period does not include the time worth of money. If a proposed investment's payback period is smaller than or equal to that of an existing solution for the same application, it may be worthwhile to pursue. If not, more investigation is required.

The concept of depreciation *d* is based upon the fact that physical facilities deteriorate and decline in usefulness with time, thus decreasing the values of the facility. There are several ways to estimate the depreciation rate, but the Modified Accelerated Cost Recovery System (MACRS) is used in this study. With MACRS, a recovery period is selected based on the type of facility and a correlation is applied. These rates are based on average recovery period by IRS 2021 [43]. For power plants, a 15-year recovery period is commonly assumed [40].

In this study, the advanced SMR system produce and sells electricity and the combined advanced SMR and ChHP produce and sell both thermal energy and electricity at natural gas and electricity prices, respectively. The cost of selling thermal (heat) energy also account for carbon tax with natural gas prices. The sales income will be different for above explained cases. For the electricity-only case, the annual sales are evaluated using the Equation 18. The assumptions used in this study for heat engine efficiency (η) to produce electricity is 34%. The capacity factor (*CF*) is assumed to be 90% based on Sabharwall et al. [29] study. $\dot{Q}_{SMR}$ is the nominal heat generated by the advanced SMR and SP_e is the selling price of electricity.

$$s_{j,SMR} = \eta \cdot CF \cdot \dot{Q}_{SMR} \cdot SP_e \cdot 8760\ hrs \tag{18}$$

For the combined advanced SMR-ChHP system, which provides and sell both electricity and heat to the market, a carbon tax was added to the natural gas prices to estimate the selling price of heat. The annual sales for the combined advanced SMR-ChHP system are given by Equation 19 where SP_{ht} is the selling price of heat (combined natural gas and carbon tax prices), $\dot{Q}_{ChHP,in}$ is the heat rate from SMR to ChHP and $\dot{Q}_{ChHP,out}$ is the rate of thermal out energy from ChHP.

$$s_{j,SMR-ChHP} = \left(\left(\eta \cdot CF \cdot (\dot{Q}_{SMR} - \dot{Q}_{ChHP,in}) \cdot SP_e\right) + \left(CF \cdot \dot{Q}_{ChHP,out} \cdot SP_{ht}\right)\right) \cdot 8760\ hrs \quad (19)$$

The annual costs are calculated using the Equation 20 where the specific and fixed cost of operation and maintenance for the advanced SMR are represented by $O\&M_{spec}$ and $O\&M_{fix}$, respectively. The specific fuel cost the uranium is represented by $Fuel_{spec}$. The values assumed for this study will be described in detail in Section 4.2. for different cases and scenarios.

$$c_0 = CF \cdot \dot{Q}_{SMR} \cdot \left(O\&M_{spec} + Fuel_{spec}\right) \cdot 8760\ hrs + \ O\&M_{fix} \cdot 1\ yr \quad (20)$$

4.1.4 Net Present Value

Net present value (NPV) also known as net present worth is the difference between the present value of cash inflows and the present value of cash outflows over the lifetime of the plant [40]. The "present" year identification is fairly arbitrary, and we chose the first year of the plant operation to be present. NPV accounts for the time value of money and is estimated using the following Equation 21.

$$NPV = \sum_{j=1}^{N} PWF_{cf,j}(A_j + rec_j) - \sum_{k=1}^{Nc} PWF_{v,k}\, ₸_k \quad (21)$$

$$PWF_{cf,j} = (1+i)^{-j} \quad (22)$$

$$PWF_{v,j} = (1+i)^{N_c - j} \quad (23)$$

The *rec* is the cost recovered from salvaged components, and ₸ is the investment cost, N_c is the construction time in years. Equation 22 represents the present worth factor for the annual cash flows. This factor discounts future cash flows where *i* is the discount rate. The same rate, *i* can be assumed for the present worth factor in Equation 23, which compounds past investments. Both factors adjust the value of the money from past or future value to the present value. The cost recovered was assumed to be zero for this analysis.

$$i = \frac{WACC+1}{r_{inf}+1} - 1 \quad (24)$$

The discount rate *i* is an interest rate that provides the current worth of future money, as shown in Equation 24 from Boldon [28]. A nominal discount rate includes inflation, while the real discount rate does not. The assumed inflation rate is expressed as r_{inf} and *WACC* is the weighted average capital cost, calculated in Equation 25. The *WACC* is a value describing the percentage of capital that must be paid to the investors, so they see the expected return on investments/assets. The *WACC* may be affected by many factors, such as political and financial risks. The C_d and C_{eq} representing the rate charged for costs of capital and equity, respectively. p_d and p_{eq} representing the portions of debt and equity for the project.

$$WACC = (p_d \times C_d) + \left(p_{eq} \times C_{eq}\right) \quad (25)$$

The portion of debt and charge rate of debt were assumed for the analysis. The portion of equity is just the portion let over that was not financed *(1-p_d)*. The rate charged for cost of equity is evaluated using the Equation 26 from Boldon [28], where Φ is the corporate tax rate that is assumed.

$$C_E = C_D(1 - \Phi) \tag{26}$$

The construction period of 3 years was assumed and constriction schedule for advanced SMR was assumed to be 60%, 20%, and 20% for 1st, 2nd, and 3rd year respectively based on study by Alonso et al. [30]. ChHP construction schedule is assumed to be 0%, 20%, and 80% for 1st, 2nd, and 3rd year respectively. The project is not considered profitable if the net present worth is negative. In making the comparisons of the investments, the larger the NPV, the more favorable is the investment.

4.1.5 Discounted Cash Flow Rate of Return

The DCFR also known as internal rate of return is the return on investment while considering the time value of money. It is obtained from an investment in which all the investment and cash flow are discounted [40]. The DCFR is estimated by making the net present worth equal to zero and solving for the rate used in the present worth factors using Equation 27. If the DCFR exceeds the WACC, the project is considered profitable.

$$0 = \sum_{j=1}^{N}\left[(1 + DCFR)^{-j}\right]\left(A_j + rec_j\right) - \sum_{k=1}^{N_c}[(1 + DCFR)^{N_c - k}]₸_k \tag{27}$$

4.1.6 Levelized Cost of Energy

The levelized cost of energy is the average cost of energy ($/MW-h or ¢/kW-h) produced over the lifetime of the plant and is calculated using Equation 28, where E_j is the energy produced each year. For this study, the LCOE is the combined cost of total electricity and thermal energy produced. It is also defined as "the discounted lifetime cost of ownership and usage of a generation asset, transformed into a $/MWh equivalent unit of cost of generation." The energy produced is discounted in LCOE calculations [44]. When comparing different investments or technologies, LCOE is best tool to employ as it measures the competitiveness of the technology. Less-competitive technology is assessed by a higher value of LCOE.

$$LCOE = \frac{\sum_{j=1}^{N} PWF_{cf,j}(c_{o,j}) + \sum_{k=1}^{Nc} PWF_{v,k}₸_k}{\sum_{j=1}^{N} PWF_{cf,j}E_j} \tag{28}$$

4.2 Study Approach and Assessment Scenarios

To study the TEA of the advanced SMR and SMR combined with ChHP, the utility data were assumed from U.S. Energy Information Administration [45] for six different regions (California, Northwest, Midwest, Southwest, New England, and PJM) of United States as shown in Table 6. The values were averaged for industrial gas prices and electricity data for the year 2021.

Table 6. Utility data for different regions.

Region	2021 Industrial Natural Gas Price ($/MMBtu)	2021 Electricity Data ($/MWh)
California	9.06	66.5
Midwest	6.07	57.7
Northwest	8.15	59.78
New England	9.68	47.75
Southwest	5.62	64.78
PJM	6.67	42.55

For this study, an advanced SMR with a thermal output 100 MW_{th} is assumed. For the TEA, different scenarios are considered based on the different thermal output of ChHP, as shown in Figure 18 for an ideal case (*CF*=100%). Scenario 1 is when the 100 MW_{th} advanced SMR sells electricity with a heat engine efficiency of 34% is represented as SMR. Scenario 2 has NHES where a 100-MW_{th} advanced SMR is coupled with 50 MW_{th} output ChHP with coefficient of performance of 0.58, which sells heat and rest of the energy from SMR sells electricity and is represented as NHES-1. In Scenario 3, NHES-2 is where the advanced SMR is coupled with 10 MW_{th} output ChHP, which offers heat and the rest of the energy from SMR produces electricity. Scenarios 4 and 5, NHES-3 and NHES-4 includes the advanced SMR coupled with 5 and 1 MW_{th} output ChHP, respectively.

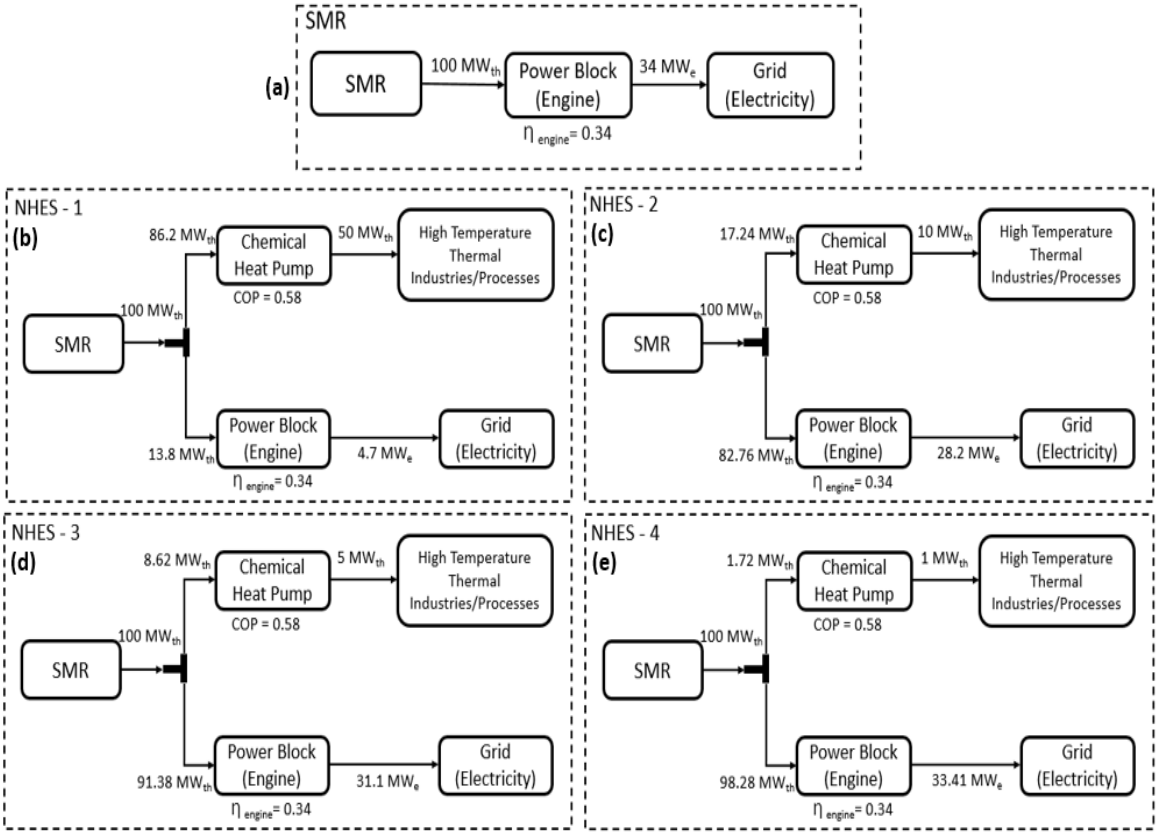

Figure 18. Advanced SMR and SMR-ChHP combined scenarios.

For conducting the economic analysis, the economic parameters assumed from the literature are listed in Table 7. Based on these assumptions and utility prices at different regions, the techno-economic study is conducted to determine the profitable scenarios for the advanced SMR and SMR coupled with ChHP with different thermal output. The economic parameters evaluated are NPV, PBP, DCFR, and LCOE to discover the potential of selling heat from the advanced SMR coupled with ChHP for high-temperature industrial processes. A parametric study based on different OCC of advanced SMR and carbon taxes is also conducted.

Table 7. Parameters assumed for this study.

Parameters	Assumed Values	References
Overnight Cap Cost	\$4,637/kW_e	Sabharwall et al. [29]
Capacity Factor	90%	Sabharwall et al. [29]
Lifetime	60 years	Sabharwall et al. [29], Alonso et al. [30]
Variable O&M Cost	\$0.486/MW_e-h	Sabharwall et al. [29]
Fixed O&M Cost	\$19,500,000/yr	Sabharwall et al. [29]
Fuel Cost	\$0 (included in O&M)	Sabharwall et al. [29]
Construction Period	3 (60%, 20%, 20%)	Alonso et al. [29]
CO_2 Tax	\$150/tonne	Locatelli et al. [46]
Depreciation	Variable	MACRS Method [33]
Corporate Tax Rate	21%	Nuclear Energy Institute [2]
Inflation Rate	1.1%	MIT report [3]
Cost of Debt	4%	Sabharwall et al. [29]
Debt Portion	30%	Sabharwall et al. [29]

4.3 Results and Discussion

In this study, based on the economic input assumptions, the calculated discount rate (i) is 3.552%, cost of equity is 4.84%, and $WACC$ is estimated to be 4.588%. ChHP-specific capital cost was estimated as \$4,500/kW based on thermal model for baseline system and the CG Thermal-specific chemical bed cost assumption [39]. These calculated values will be used to determine the economic parameters and profitability of the different scenarios between advanced SMR and SMR-ChHP systems.

4.3.1 Economic Parameters Analysis

Based on the utility prices assumed for six different U.S. regions, economic parameters for SMR, NHES-1, NHES-2, NHES-3, and NHES-4 were evaluated, as described in Section 4.2. Figure 19 shows the NPV values of advanced SMR and SMR-ChHP output scenarios. All the NHESs have the higher NPV values then SMR for every region because of higher sales revenue. As per NPV estimates, it is observed that selling heat from NHES-1 with a ChHP thermal out of 50 MW_{th} is most profitable compared with lower thermal output ChHP or selling electricity from 100 MW_{th} advanced SMR. The New England and PJM regions' NPV values of $162M and $251.8M show the best case for selling heat for high-temperature industrial processes because of their high natural gas and low electricity prices as per the percentage increase in NPV values compared with SMR in their region.

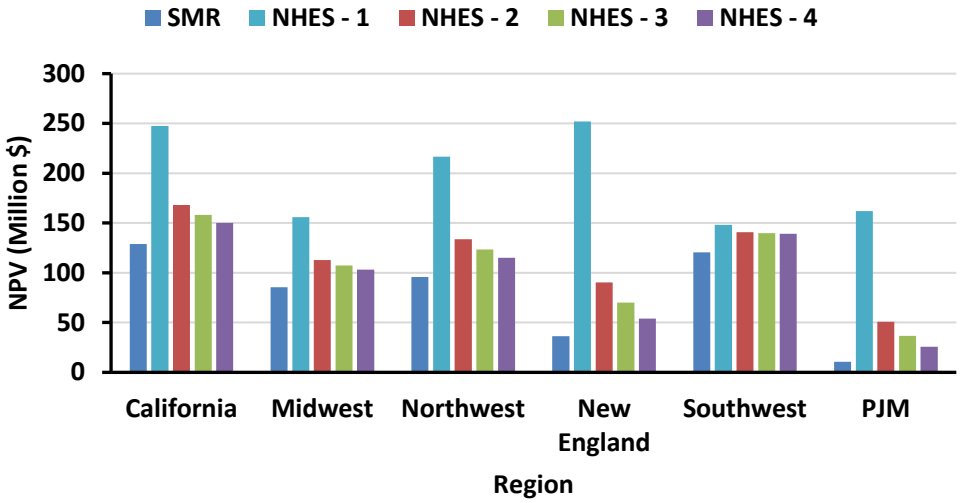

Figure 19. NPV values at different regions for SMR and different SMR-ChHP output scenarios.

Figure 20 shows the payback period (PBP) of advanced SMR and SMR-ChHP output scenarios and Figure 21 shows the percentage deviation of PBP for different NHES systems from advanced SMR values. The New England and PJM regions showed a shorter payback period of 16.4 and 19.12 years, respectively, for NHES-1 making the most profitable scenario for selling heat at higher scale, whereas for other regions PBP for NHES-1 system were higher. NHES-2, 3, and 4 showed slightly lower PBP from advanced SMR values in the California, Midwest, Northwest, and Southwest regions. NHES-4 is the most profitable case in the California, Midwest, Northwest, and Southwest regions as the PBP period is the lowest among NHES-2 and 3 and advanced SMR asserting that SMR coupled with 1 MW_{th} ChHP system providing heat and electricity is always profitable than advanced SMR selling electricity only in terms of PBP calculations. The negative percentage deviation in Figure 10 shows the PBP of NHES system is lower than advanced SMR values making system profitable. Except NHES-1 in the California, Southwest, Northwest, and Southwest regions, NHES-2 in the Southwest have positive percentage deviation from SMR values favoring SMR. Even though the ChHP has higher sales income and NPV values, the NPV is computed by making an assumption of 60-year plant life, which means after the capital cost is recovered there are many years to earn a profit.

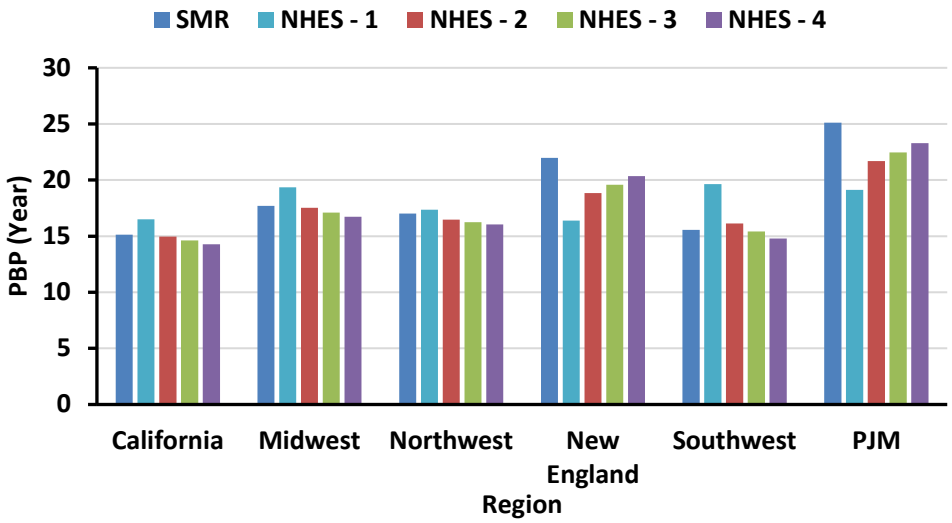

Figure 20. PBP at different regions for SMR and different SMR-ChHP output scenarios.

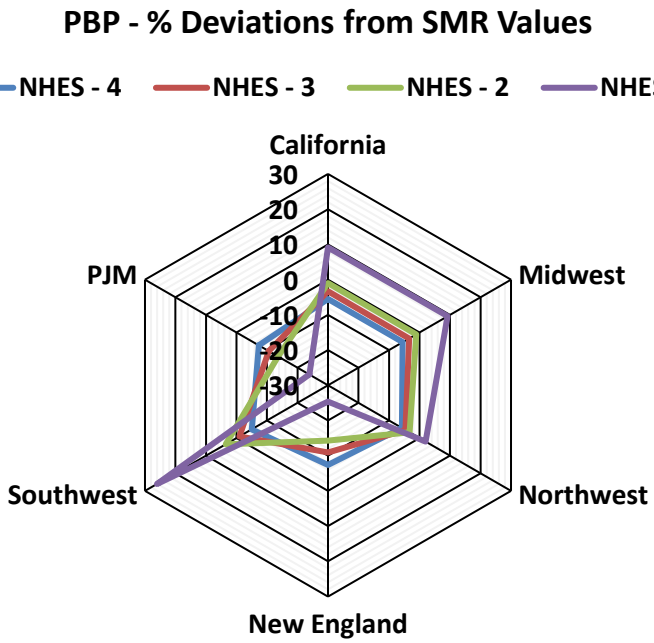

Figure 21. Percentage deviation of PBP for different NHES scenarios from SMR values.

Figure 22 shows that the DCFR calculations and all the NHES systems have DCFR values greater than WACC, asserting the project is acceptable, which should be compared with other accepted scenarios or projects as per Bolden 2015 [27]. The DCFR values for New England and PJM are significant higher for NHES-1 system compared with advanced SMR making it the most profitable case for selling heat. Figure 23 shows the percentage deviation of DCFR for different NHES systems from advanced SMR values. The four cases where DCFR values of NHES systems are less than advanced, the SMR values are California, Midwest, and Southwest for NHES-1 system, and NHES-2 for the Southwest system. The DCFR analysis also confirmed that SMR-ChHP system is always profitable at different regions based on different ChHP thermal output scenarios.

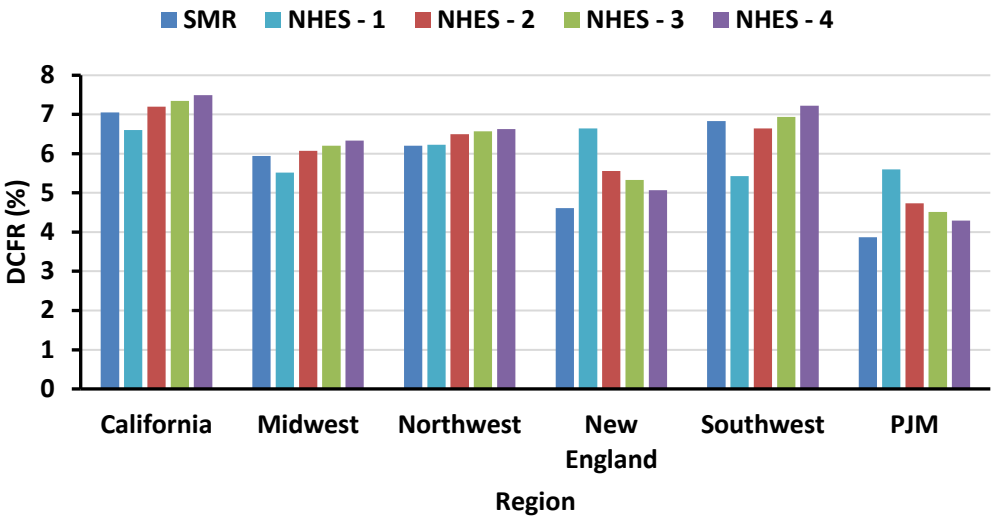

Figure 22. DCFR at different regions for SMR and different SMR-ChHP output scenarios.

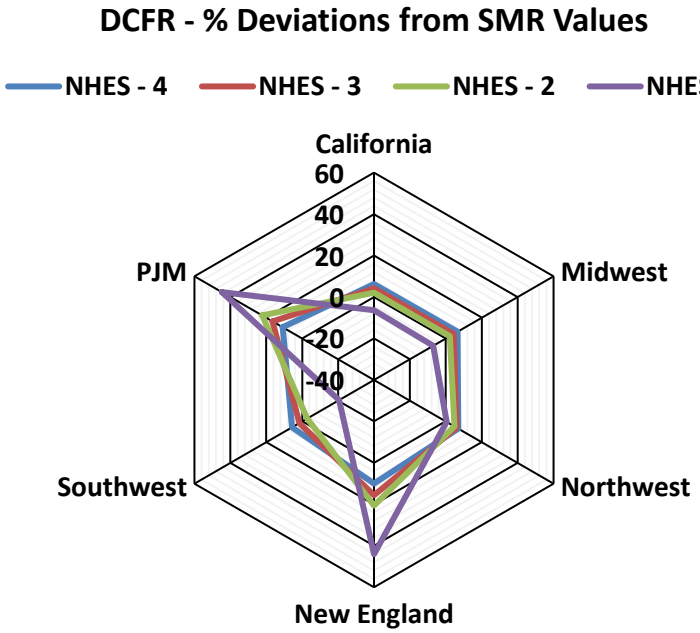

Figure 23. Percentage deviation of DCFR for different NHES scenarios from SMR values.

The Figure 24 shows the LCOE values for SMR and NHES systems for different scenarios. The LCOE for advanced SMR is 36.93 $/MWh whereas the different coupled SMR-ChHP scenarios have LCOE values 23.85, 36.14, 38.62 and 40.88 $/MWh for NHES-1, 2, 3, and 4, respectively. NHES-1 has lower LCOE when compared to advanced SMR making NHES-1 a better investment as SMR-ChHP system is producing more energy than advanced SMR and overcomes the cost of the coupled system well. NHES-2 has slightly higher LCOE value compared to advanced SMR signifying that selling heat and electricity via coupled system balances out the cost of SMR-ChHP. NHES-3 and 4 have higher LCOE as the cost of the system does not balances out the energy produced by the coupled system.

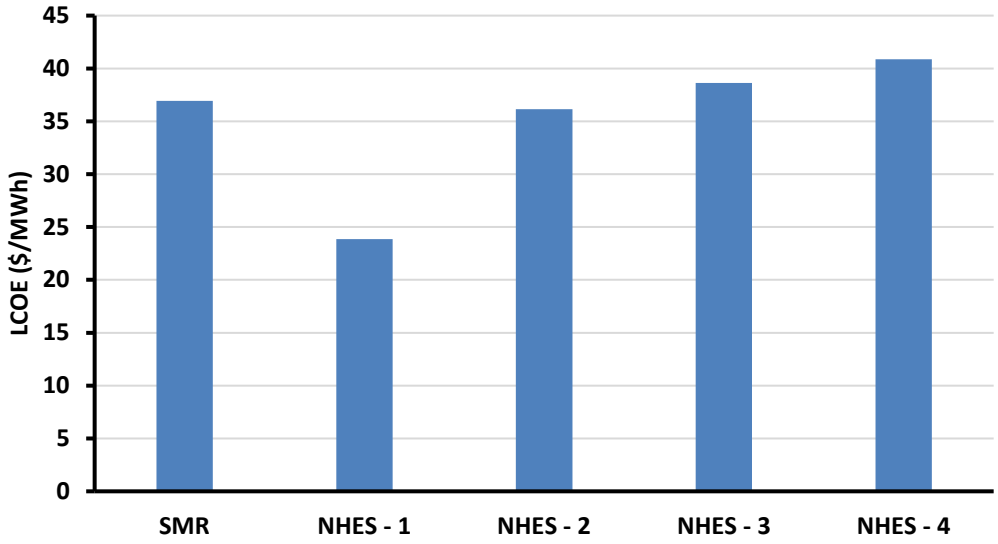

Figure 24. LCOE for SMR and different SMR-ChHP output scenarios.

Based on the above evaluated economic parameters for different U.S. region, nuclear hybrid energy system comparing of SMR coupled with ChHP showed that selling heat to high-temperature industrial process and electricity to the grid makes advanced SMR more profitable and helps reducing the burning of fossil fuels to produce heat. In the California, Midwest, Northwest, and Southwest regions, it is more profitable to have NHES-3 or 4 compared with NHES-1 and 2 and advanced SMR based on PBP and DCFR values. Though based on high NPV values, NHES-1 can also be considered. In PJM and New England, NHES-1 is more profitable based on their utility prices, asserting selling heat at higher scale is more cost-effective and favorable.

4.3.2 Parametric Study on Overnight Capital Cost of Advanced SMR

To access the economic competitiveness of advanced SMR and different SMR-ChHP systems, a parametric study on OCC of advanced SMR is conducted for the values ranging from \$4500/kW_e to \$6,500/kW_e based on the diverse values reported in literature. The aim of this parametric study is to assess the effect on NPV and PBP of the proposed scenarios for different utility prices and U.S. regions. Advanced SMR, NHES-1, and NHES-2 will be the focus of this study based on results discussed in Section 4.3.1.

Figure 25, 26, 27, and 28 show the NPV and PBP values at different OCC of advanced SMR for California, Midwest, Northwest, and Southwest, respectively. As the OCC of advanced SMR is increased the NPV of the SMR, NHES-1 and 2 decreased as expected with increase in PBP. For the California, Midwest, Northwest, and Southwest regions, NPV of NHES-1 and 2 are still positive and higher than advanced SMR value when the OCC of advanced SMR is increased from \$4500/kW_e to \$6,500/kW_e.

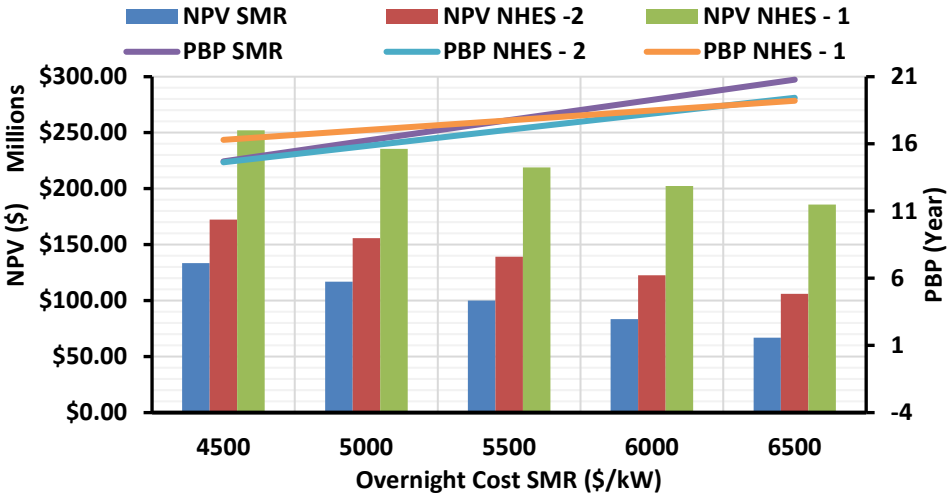

Figure 25. NPV and PBP versus overnight cost of advanced SMR for the California region.

For California, the PBP starts to get lower for NHES-2 and NHES-1 when compared with advanced SMR once the OCC of SMR is more than \$5,500/kW_e and \$6,100/kW_e, respectively. Based on utility data from the Midwest region, the PBP of NHES-2 and NHES-1 when compared with advanced SMR begins to reduce once the OCC of SMR is increased to \$4,500/kW_e and \$5,500/kW_e, respectively. The PBP for the Northwest region was already less for NHES-1 when compared with SMR for \$4,500/kW_e OCC. When the OCC is increased to \$4,800/kW_e the NHES-1 system had less PBP then advanced SMR. The Southwest region, NHES-1 would not have lower PBP than advanced SMR based on assumed OCC. NHES-2 will have PBP lower than advanced SMR once the OCC is increased to \$5,800/kW_e.

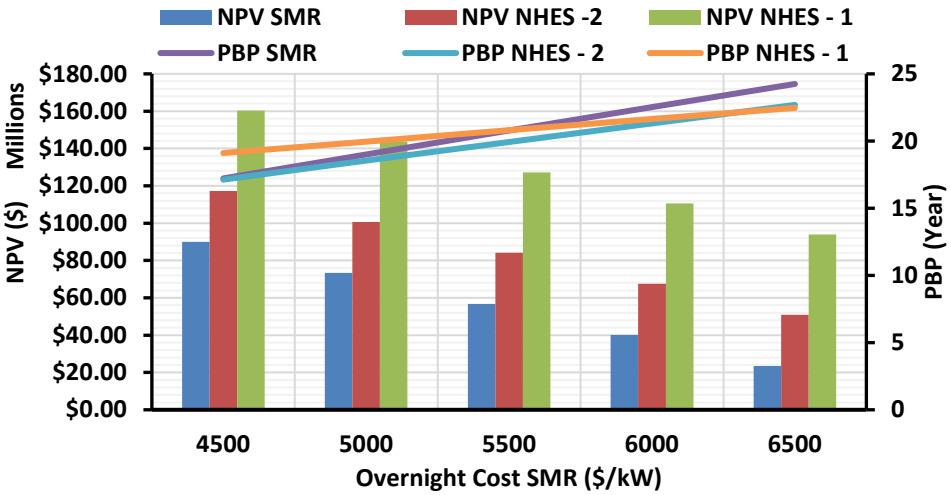

Figure 25. NPV and PBP versus overnight cost of advanced SMR for the Midwest region.

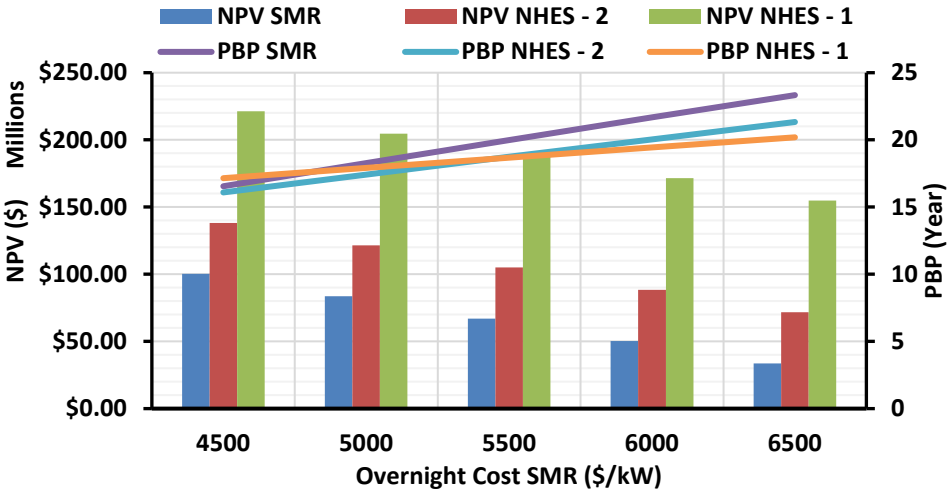

Figure 26. NPV and PBP versus overnight cost of advanced SMR for the Northwest region.

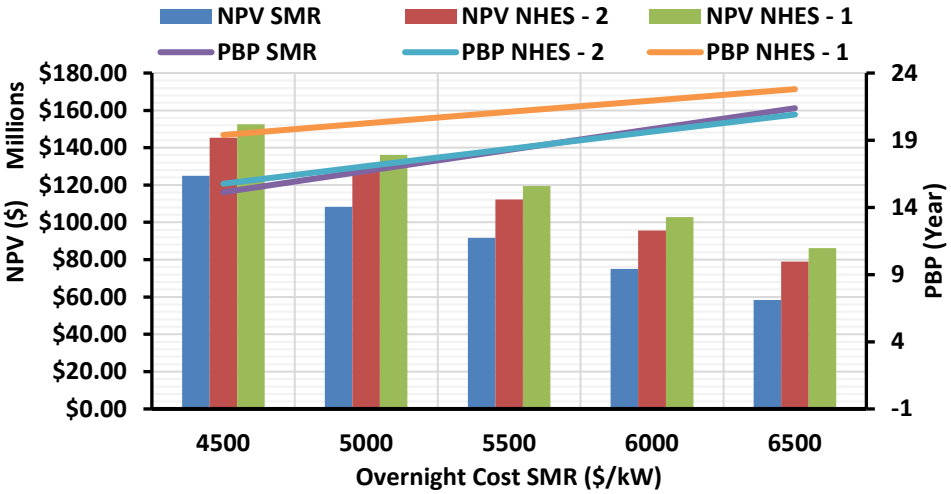

Figure 27. NPV and PBP versus overnight cost of advanced SMR for Southwest region.

Figures 29 and 30 show the NPV and PBP values at different OCC of advanced SMR for New England and PJM, respectively. Based on the New England and PJM utility prices, NHES-1 will always shave lower PBP when compared with NHES-2 and advanced SMR with increased OCC though the individual system PBP value will increase. NPV of both the regions are significantly higher for NHES-1. If the OCC is increased above \$5,500/kW_e and \$5,000/kW_e for New England and PJM, respectively, then NPV of SMR will become negative making SMR not profitable. In this case, the system will be economic profitable if SMR is coupled with ChHP and sells heat and electricity.

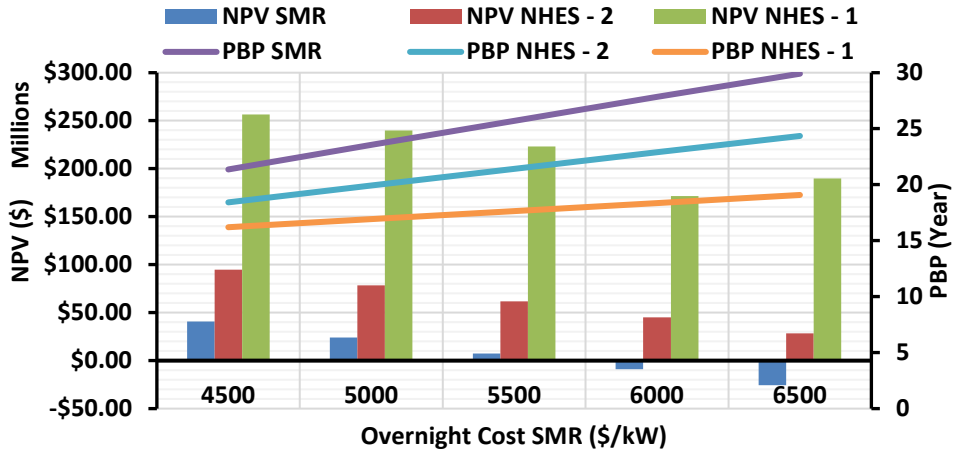

Figure 29. NPV and PBP versus overnight cost of advanced SMR for the New England region.

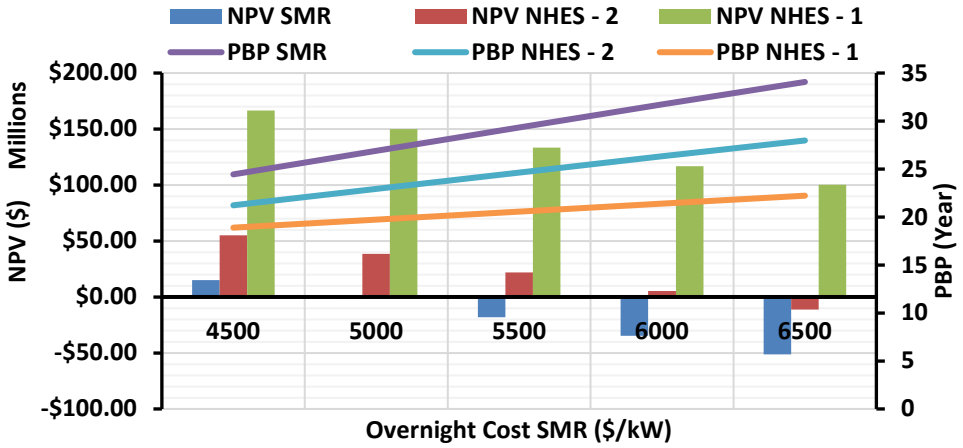

Figure 28. NPV and PBP versus overnight cost of advanced SMR for the PJM region.

4.3.3 Impact of Increased Carbon Taxes

The goal to prevent global temperature from rising above 1.5°C by 2030, which was committed at COP26, the price of carbon tax should be higher. This tax reduces emissions in two ways. First, increasing the cost of carbon-based fuels will motivate to switch to clean energy technologies, such as nuclear, solar, wind, and hydro sources. Taxes will allow industries to find most cost-effective way to reduce emissions, which is a better alternative to free-market economies than government regulation. This study was conducted to analyze the impact of increased carbon taxes on PBP for NHES (SMR-ChHP) systems.

The two-carbon tax rates were assumed in this study (e.g., $150/tonne) (which was assumed in Section 4.3.1) and $200/tonne. As carbon tax rate will impact the heat value that is why different NHES scenarios are studied for different U.S. regions. All the assumption were unchanged except carbon tax. As NPVs of the NHES systems were significantly higher than advanced SMR for all the scenarios and cases, PBP was the focus of this study. For the California region, the percentage deviation of PBP with different

carbon taxes were shown in Figure 31 for different NHES systems when compared with advanced SMR. When carbon tax of $150/tonne was assumed, NHES-1 had 9.1% higher PBP than advanced SMR but as the carbon tax increased to $200/tonne the PBP was reduced to -3.5% than advanced SMR. PBP of NHES-2, 3, and 4 systems were further lowered than advanced SMR values when carbon tax were increased to $150/tonne to $200/tonne. Similar trend was followed by the Midwest region as shown in Figure 32 where PBP of NHES-2, 3 and 4 systems were further lowered than advanced SMR values when carbon tax were increased. Whereas the NHES-1 had 9.2% higher payback period compared with SMR value at $150/tonne carbon tax and this value was lowered to -5.4% when carbon tax was increased to $200/tonne.

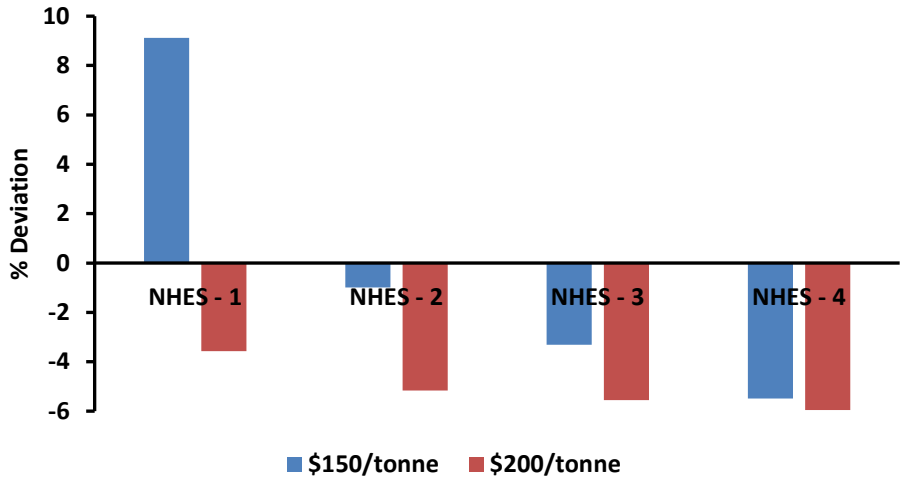

Figure 29. Percentage deviation in PBP based on increased carbon tax for the California region.

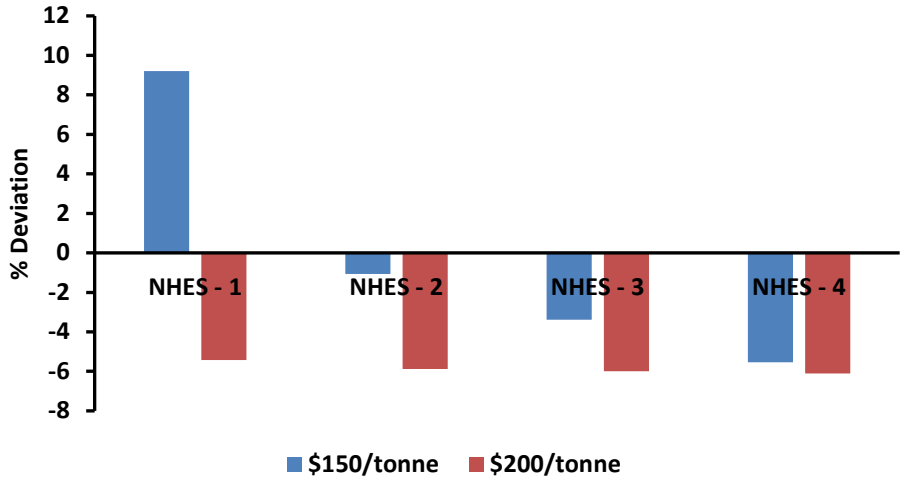

Figure 30. Percentage deviation in PBP based on increased carbon tax for the Midwest region.

For the Northwest region, the percentage deviation in PBP values for NHES-2, 3, and 4 were further lowered as excepted compared with SMR when carbon tax was increased as shown in Figure 33. But for NHES-1, the PBP was 2% higher and was reduced to -10.45% compared with SMR when the carbon tax was increased from $150/tonne to $200/tonne, respectively. In the Southwest region, as shown in Figure 34, even after increasing the carbon tax to $200/tonne, PBP of NHES-1 was still higher than

advanced SMR value. Though PBP of NHES-2, 3, and 4 systems were lowered than SMR values with increased carbon tax.

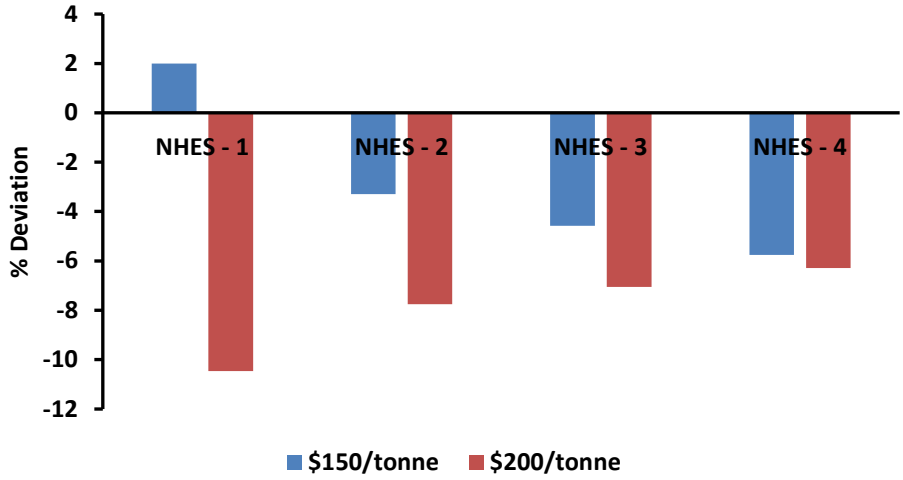

Figure 31. Percentage deviation in PBP based on increased carbon tax for the Northwest region.

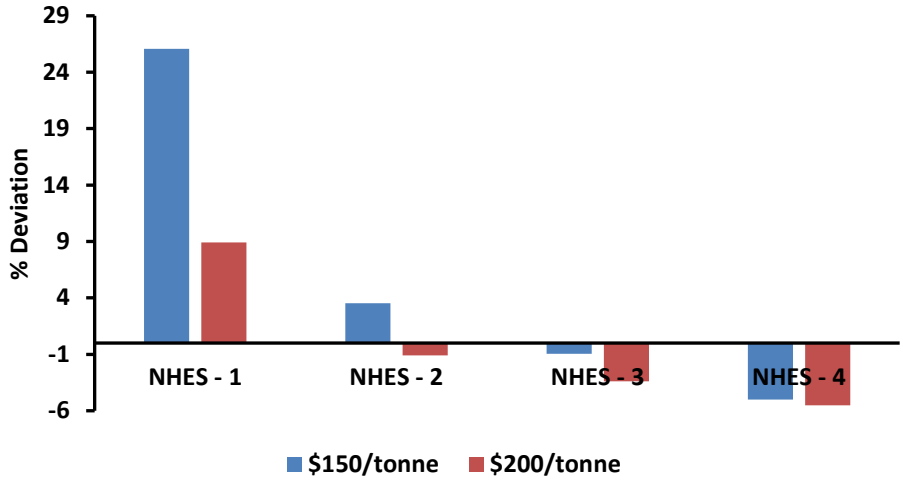

Figure 32. Percentage deviation in PBP based on increased carbon tax for the Southwest region.

The New England and PJM were the two most profitable cases for the NHES-1 system as per the study described in Section 4.3.1. Increasing the carbon tax rate has further lowered the PBP from -25.35% to -34.04% and -22.88% to -34% from SMR values for New England and PJM regions, respectively, as shown in Figure 35 and Figure 36.

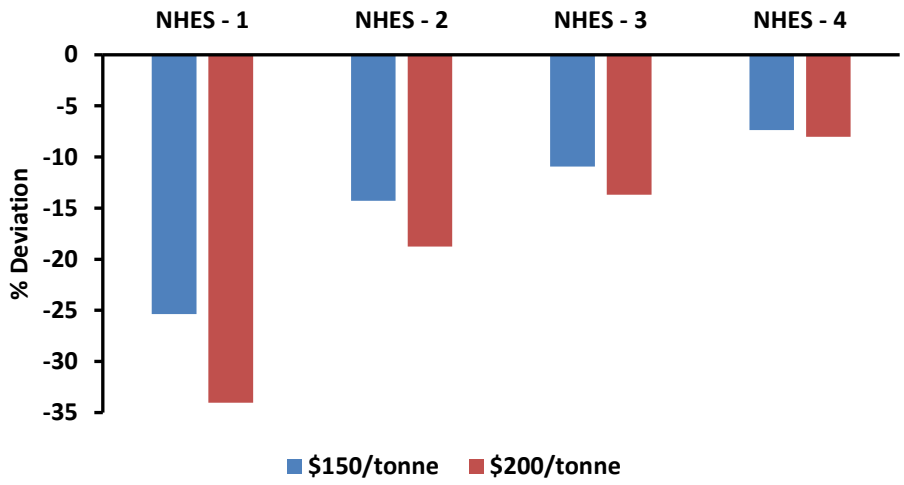

Figure 33. Percentage deviation in PBP based on increased carbon tax for the New England region.

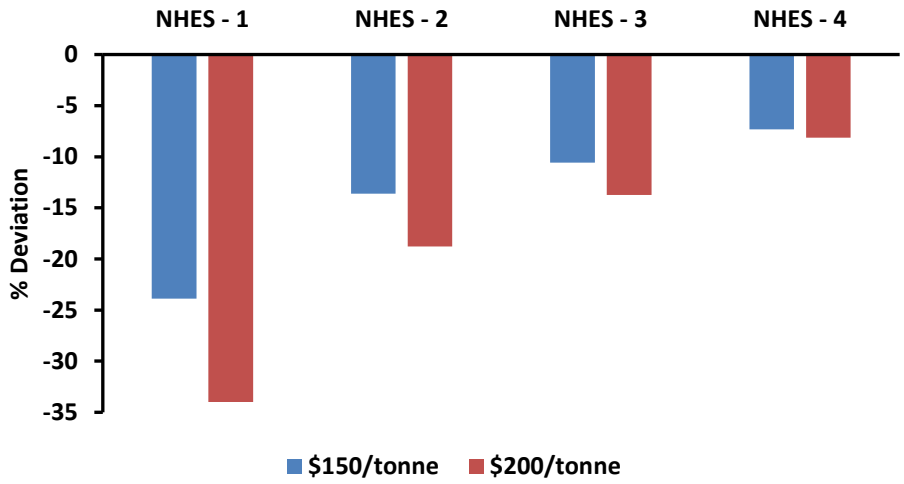

Figure 34. Percentage deviation in PBP based on increased carbon tax for the PJM region.

5. CONCLUSIONS

A steady state model was built to develop a ChHP capital cost system for pilot-scale (25-, 100-, and 1000-kW) study. A TEA was conducted for advanced SMR and SMR coupled with different thermal output ChHP system to determine the profitability of selling heat rather than electricity only. A steady-state thermal model of ChHP was used for TEA. The electricity and natural gas prices were assumed for six different U.S. regions (California, Northwest, Midwest, Southwest, New England, and PJM) based on Energy Information Administration data. For this study, advanced SMR, combined with ChHP, was referred as NHES. Advanced SMR with 100 MW_{th} and four different scenarios of NHES were considered based on thermal output from ChHP (e.g., 50-, 10-, 5-, and 1-MW_{th} represented as NHES-1, 2, 3, and 4, respectively). The NPV, PBP, DCFR, and LCOE were evaluated for SMR and NHES systems. The economic analysis showed that selling heat and electricity from SMR-ChHP is profitable in most cases based on utility prices of different regions. The parametric study on increasing OCC of advanced SMRs indicated selling heat will be economically profitable than selling only electricity. Increased carbon tax also showed a significant improvement in economic parameters for configurations involving selling heat.

Providing heat to the high-temperature thermal industries could be a game changer for nuclear power and help achieve the climate change goal by reducing the burning of fossil fuel.

5.1 Future Work and Considerations

A TEA on hourly utility data for different U.S. regions will be valuable to understand the combination of electricity and high-temperature heat produced. Further research and development on the ChHP and chemical bed design are essential for reduction in the specific capital cost of ChHP system. Market analysis on high-temperature industrial power required is necessary to understand the possible scale of the system.

6. REFERENCES

1. C. Forsberg, S. Brick, and G. Haratyk. 2018. "Coupling heat storage to nuclear reactors for variable electricity output with baseload reactor operation," *The Electricity Journal* 31: 23–31. https://doi.org/10.1016/j.tej.2018.03.008.
2. NEI, "Cost Competitiveness of Micro-Reactors for Remote Markets" Nuclear Energy Institute. April 15, 2019. https://www.nei.org/resources/reports-briefs/cost-competitiveness-micro-reactors-remote-markets (accessed November 21, 2021).
3. J. Buongiorno, M. Corradini, J. Parsons, D. Petti. 2018. "The Future of Nuclear Energy in a Carbon-Constrained World," MIT, IEEE, vol. 275.
4. IAEA. 2020. "Advances in Small Modular Reactor Technology Developments A Supplement to: IAEA Advanced Reactors Information System (ARIS) 2020 Edition," *International Atomic Energy Agency (IAEA)*.
5. S. M. Bragg-Sitton, R. Boardman, C. Rabiti, and J. O'Brien. 2020. "Reimagining future energy systems: Overview of the US program to maximize energy utilization via integrated nuclear-renewable energy systems," *International Journal of Energy Research* 44:8156–8169. https://doi.org/10.1002/er.5207.
6. S. M. Bragg-Sitton, R. Boardman, C. Rabiti, J. Suk Kim, M. McKellar, P. Sabharwall, J. Chen, M. S. Cetiner, T. J. Harrison, and A. L. Qualls. 2016. "Nuclear-Renewable Hybrid Energy Systems: 2016 Technology Development Program Plan," INL/EXT-16-38165, Idaho National Laboratory, Idaho Falls, Idaho (United States); Oak Ridge National Laboratory, Oak Ridge, Tennessee (United States). https://doi.org/10.2172/1333006.
7. C. McMillan and M. Ruth. 2016. "Generation and Use of Thermal Energy in the U.S. Industrial Sector and Opportunities to Reduce its Carbon Emissions," INL/EXT-16-39680, Idaho National Laboratory. https://doi:10.2172/1334495.
8. W. Wongsuwan, S. Kumar, P. Neveu, and F. Meunier. 2021. "A review of chemical heat pump technology and applications." *Applied Thermal Engineering* 21:1489–1519. https://doi.org/10.1016/S1359-4311(01)00022-9.
9. M. Arjmand, L. Liu, and I. Neretnieks. 2013. "Exergetic efficiency of high-temperature-lift chemical heat pump (CHP) based on CaO/CO_2 and CaO/H_2O working pairs." *International Journal of Energy Research* 37:1122–1131. https://doi.org/10.1002/er.2918.
10. P. Sabharwall, D. Wendt, and V. P. Utgikar. 2013. "Application of Chemical Heat Pumps for Temperature Amplification in Nuclear Hybrid Energy Systems for Synthetic Transportation Fuel Production," INL/EXT-13-30463, Idaho National Laboratory. https://doi:10.2172/1104502.

11. F. Schaube, L. Koch, A. Wörner, and H. Müller-Steinhagen. 2012. "A thermodynamic and kinetic study of the de- and rehydration of $Ca(OH)_2$ at high H_2O partial pressures for thermo-chemical heat storage," *Thermochimica Acta.* 538:9–20. https://doi.org/10.1016/j.tca.2012.03.003.

12. H. Matsuda, T. Ishizu, S. K. Lee, and M. Hasatani. 1985. "Kinetic study of $Ca(OH)_2$/CaO reversible thermochemical reaction for thermal energy storage by means of chemical reaction," *Kagaku Kogaku Ronbunshu* 11:542–548. https://doi.org/10.1252/kakoronbunshu.11.542.

13. L. Dai, X. -F. Long, B. Lou, and J. Wu. 2018. "Thermal cycling stability of thermochemical energy storage system $Ca(OH)_2$/CaO," *Applied Thermal Engineering* 133:261–268. https://doi.org/10.1016/j.applthermaleng.2018.01.059.

14. M. Schmidt, A. Gutierrez, and M. Linder. 2017. "Thermochemical energy storage with CaO/$Ca(OH)_2$ – Experimental investigation of the thermal capability at low vapor pressures in a lab scale reactor," *Applied Energy* 188:672–681. https://doi.org/10.1016/j.apenergy.2016.11.023.

15. M. Schmidt, C. Szczukowski, C. Roßkopf, M. Linder, and A. Wörner. 2014. "Experimental results of a 10 kW high temperature thermochemical storage reactor based on calcium hydroxide," *Applied Thermal Engineering* 62:553–559. https://doi.org/10.1016/j.applthermaleng.2013.09.020.

16. Y. A. Criado, M. Alonso, J. C. Abanades, and Z. Anxionnaz-Minvielle. 2014. "Conceptual process design of a CaO/$Ca(OH)_2$ thermochemical energy storage system using fluidized bed reactors," *Applied Thermal Engineering* 73:1087–1094. https://doi.org/10.1016/j.applthermaleng.2014.08.065.

17. F. Schaube, A. Kohzer, J. Schütz, A. Wörner, and H. Müller-Steinhagen. 2013. "De- and rehydration of $Ca(OH)_2$ in a reactor with direct heat transfer for thermo-chemical heat storage. Part A: Experimental results," *Chemical Engineering Research and Design* 91:856–864. https://doi.org/10.1016/j.cherd.2012.09.020.

18. S. Funayama, H. Takasu, M. Zamengo, J. Kariya, S. T. Kim, and Y. Kato. 2019. "Composite material for high-temperature thermochemical energy storage using calcium hydroxide and ceramic foam," *Energy Storage* 1:e53. https://doi.org/10.1002/est2.53.

19. A. Gupta, P. D. Armatis, P. Sabharwall, B. M. Fronk, and V. Utgikar. 2021. "Thermodynamics of $Ca(OH)_2$/CaO reversible reaction: Refinement of reaction equilibrium and implications for operation of chemical heat pump," *Chemical Engineering Science* 230:116227. https://doi.org/10.1016/j.ces.2020.116227.

20. A. Gupta, P. D. Armatis, P. Sabharwall, B. M. Fronk, and V. Utgikar. 2021. "Energy and exergy analysis of $Ca(OH)_2$/CaO dehydration-hydration chemical heat pump system: Effect of reaction temperature," *Journal of Energy Storage* 39:102633. https://doi.org/10.1016/j.est.2021.102633.

21. Y. A. Criado, M. Alonso, and J. C. Abanades. 2016. "Enhancement of a CaO/$Ca(OH)_2$ based material for thermochemical energy storage," *Solar Energy* 135:800–809. https://doi.org/10.1016/j.solener.2016.06.056.

22. J. Yan and C. Y. Zhao. 2014. "First-principle study of CaO/$Ca(OH)_2$ thermochemical energy storage system by Li or Mg cation doping," *Chemical Engineering Science* 117:293–300. https://doi.org/10.1016/j.ces.2014.07.007.

23. K. G. Sakellariou, G. Karagiannakis, Y. A. Criado, and A. G. Konstandopoulos. 2015. "Calcium oxide based materials for thermochemical heat storage in concentrated solar power plants," *Solar Energy* 122:215–230. https://doi.org/10.1016/j.solener.2015.08.011.

24. C. Roßkopf, M. Haas, A. Faik, M. Linder, and A. Wörner. 2014. "Improving powder bed properties for thermochemical storage by adding nanoparticles," *Energy Conversion and Management* 86:93–98. https://doi.org/10.1016/j.enconman.2014.05.017.

25. C. Roßkopf, S. Afflerbach, M. Schmidt, B. Görtz, T. Kowald, M. Linder, and R. Trettin. 2015. "Investigations of nano coated calcium hydroxide cycled in a thermochemical heat storage," *Energy Conversion and Management* 97:94–102. https://doi.org/10.1016/j.enconman.2015.03.034.

26. A. Gupta, P. D. Armatis, P. Sabharwall, B. M. Fronk, and V. Utgikar. 2021. "Kinetics of $Ca(OH)_2$ decomposition in pure $Ca(OH)_2$ and $Ca(OH)_2$-$CaTiO_3$ composite pellets for application in thermochemical energy storage system," *Chemical Engineering Science* 246:116986. https://doi.org/10.1016/j.ces.2021.116986.

27. L. Boldon. 2015. "Sustainability Efficiency Factor: Measuring Sustainability in Advanced Energy Systems through Exergy, Exergoeconomic, Life Cycle, and Economic Analyses," PhD Thesis, Rensselaer Polytechnic Institute. https://ui.adsabs.harvard.edu/abs/2015PhDT.....258B (accessed March 1, 2022).

28. L. M. Boldon and P. Sabharwall. 2014. "Small modular reactor: First-of-a-Kind (FOAK) and Nth-of-a-Kind (NOAK) Economic Analysis," INL/EXT-14-32616, Idaho National Laboratory. https://doi.org/10.2172/1167545.

29. P. Sabharwall, S. Bragg-Sitton, L. Boldon, and S. Blumsack. 2015. "Nuclear Renewable Energy Integration: An Economic Case Study," *The Electricity Journal* 28:85–95. https://doi.org/10.1016/j.tej.2015.09.003.

30. G. Alonso, S. Bilbao, and E. del Valle. 2016. "Economic competitiveness of small modular reactors versus coal and combined cycle plants," *Energy* 116:867–879. https://doi.org/10.1016/j.energy.2016.10.030.

31. S. Spoelstra, W. G. Haije, and J. W. Dijkstra. 2002. "Techno-economic feasibility of high-temperature high-lift chemical heat pumps for upgrading industrial waste heat," *Applied Thermal Engineering* 22:1619–1630. https://doi.org/10.1016/S1359-4311(02)00077-7.

32. F. Karaca, O. Kıncay, and E. Bolat. 2002. "Economic analysis and comparison of chemical heat pump systems," *Applied Thermal Engineering* 22:1789–1799. https://doi.org/10.1016/S1359-4311(02)00078-9.

33. A. Bayon, R. Bader, M. Jafarian, L. Fedunik-Hofman, Y. Sun, J. Hinkley, S. Miller, and W. Lipiński. 2018. "Techno-economic assessment of solid–gas thermochemical energy storage systems for solar thermal power applications," *Energy* 149:473–484. https://doi.org/10.1016/j.energy.2017.11.084.

34. M. Linder, Chr. Roßkopf, M. Schmidt, and A. Wörner. 2014. "Thermochemical Energy Storage in kW-scale based on $CaO/Ca(OH)_2$," *Energy Procedia* 49:888–897. https://doi.org/10.1016/j.egypro.2014.03.096.

35. M. Angerer, M. Becker, S. Härzschel, K. Kröper, S. Gleis, A. Vandersickel, and H. Spliethoff. 2018. "Design of a MW-scale thermo-chemical energy storage reactor," *Energy Reports* 4:507–519. https://doi.org/10.1016/j.egyr.2018.07.005.

36. M. Schmidt, M. Gollsch, F. Giger, M. Grün, and M. Linder. 2016. "Development of a moving bed pilot plant for thermochemical energy storage with $CaO/Ca(OH)_2$," *AIP Conference Proceedings* 1734:050041. https://doi.org/10.1063/1.4949139.

37. A. Cosquillo Mejia, S. Afflerbach, M. Linder, and M. Schmidt. 2020. "Experimental analysis of encapsulated $CaO/Ca(OH)_2$ granules as thermochemical storage in a novel moving bed reactor," *Applied Thermal Engineering* 169:114961. https://doi.org/10.1016/j.applthermaleng.2020.114961.

38. P. D. Armatis, A. Gupta, P. Sabharwall, V. Utgikar, and B. M. Fronk. 2021. "A chemical-absorption heat pump for utilization of nuclear power in high temperature industrial processes," *International Journal of Energy Research* 45:14612–14629. https://doi.org/10.1002/er.6721.

39. Graphite & SIC Heat Exchangers | Fluoropolymers | CG Thermal. 2022. https://cgthermal.com/ (accessed March 1, 2022).

40. P. M. Timmerhaus, K. D. West, and P. Ronald. 2003. *Plant Design and Economics for Chemical Engineers*, Fifth Edition. McGrawl-Hill.

41. J. Richards, P. Sabharwall, and M. Memmott. 2017. "Economic comparison of current electricity generating technologies and advanced nuclear options," *The Electricity Journal* 30:73–79. https://doi.org/10.1016/j.tej.2017.11.005.

42. W. R. Stewart, and K. Shirvan. 2022. "Capital cost estimation for advanced nuclear power plants," *Renewable and Sustainable Energy Reviews* 155:111880. https://doi.org/10.1016/j.rser.2021.111880.

43. IRS. 2020. Publication 946, *How To Depreciate Property*. https://www.irs.gov/publications/p946 (accessed March 1, 2022).

44. J. Aldersey-Williams and T. Rubert. 2019. "Levelised cost of energy – A theoretical justification and critical assessment," *Energy Policy* 124:169–179. https://doi.org/10.1016/j.enpol.2018.10.004.

45. EIA. 2022. *U.S. Energy Information Administration*. https://www.eia.gov/index.php (accessed March 1, 2022).

46. G. Locatelli, C. Bingham, and M. Mancini. 2014. "Small modular reactors: A comprehensive overview of their economics and strategic aspects," *Progress in Nuclear Energy* 73:75–85. https://doi.org/10.1016/j.pnucene.2014.01.010.